Wave power trends along the U.S. coastline: in situ measurements and model hindcast estimates

Candice Hall[1,2] · Robert E. Jensen[1] · David W. Wang[3]

Abstract

Observational data are successfully assessed to investigate wave power (wave energy flux per unit of wave-crest) trends within four coastal regions around the US, a parameter that is deemed vital to those responsible for coastal protection and community resilience. This study tests for shifting observational inter-annual wave power trends using a newly developed, unique, United States Army Corps of Engineers Quality Controlled Consistent Measurement Archive, and offers a viable methodology to remove documented observational time series data discontinuations. This study is one of the first to show spatially and temporally comparative observational and model wave power results, providing new information on the accuracy of model wave power estimates, while showcasing in situ wave power trends at 29 sites around the U.S. coastline. Overall, the majority of the eastern Pacific Ocean and Hawaii wave power trends are downward, with mixed slope wave power trends apparent within the Atlantic Ocean and the Gulf of Mexico. Observational and model results are similar with respect to timing, but not magnitude, of wave power peaks in long-term inter-annual trends, with the moored buoy data presenting smaller wave power ranges for two (eastern Pacific Ocean and Hawaii) of the four regions. Additionally, the detection of a noticeable variability in the wave power trend direction within each region suggests that site-specific wave power trends should not be generalised to represent a large region. This work demonstrates that observational data are essential in local and regional wave climate studies to accurately estimate wave power for coastal planners and engineers.

Keywords Wave power · Wave energy flux · Wave system · Nonstationary resource trend · Moored buoys · USACE QCC Archive · United States

1 Introduction

Wave power measures the transport of wave energy (wave energy flux per unit of wave-crest) that is critical for shoreline evolution. Huppert et al. (2020) showed that wave power is a good predictor of how fast or slow a rocky coastline of Hawaii will erode, while Suzuki and Yoshiaki (2018) demonstrated that medium-term shoreline fluctuation is a direct result of wave power influence. Leonardi et al. (2015) postulate that variations in the background or mean wave power over the long term appear to have a greater effect on salt marsh erosion than short-term extreme wave conditions. Therefore, the background wave climate and associated long-term inter-annual wave power trends are critically important for engineers to design, protect and fortify our coastal infrastructure (USACE, 2002).

There has been a substantial effort in the impact of extreme storm events and the wave heights that affect our coastlines (Massey et al., 2011; Cialone et al., 2015; Gravens et al., 2018; Massey 2019). As multiple studies show that wave heights are increasing over time (Allan and Komar, 2000; Komar and Allan, 2007; Menéndez et al. 2008; Ruggiero et al., 2010; Young et al., 2011; Bertin et al., 2013; Panchang et al., 2013; Storlazzi et al., 2015; Jabbari et al., 2021), then it stands to reason that the power of the waves hitting our coastlines is increasing. Monitoring events and/or peak conditions from a storm might not track mean coastal damage or climate trends sufficiently, as a modest event lasting hours or days could have a larger impact on a coastline

✉ Candice Hall
candice.hall@usace.army.mil

[1] USACE Engineer Research and Development Center, Vicksburg, MS, USA

[2] Department of Oceanography, University of Cape Town, Cape Town, South Africa

[3] Naval Research Laboratory, Stennis Space Center, MS, USA

than a fast-moving extreme event. For instance, Panchang et al. (2013) and Appendini et al. (2018) found that although maximum significant wave height did not increase significantly in their independent Gulf of Mexico studies, the frequency of larger waves did. Therefore, with the added scaling effects of larger waves (with larger waves, the wavelength and period must increase), the use of only one variable (height) would lead to inaccurate results. These results necessitate an understanding of the background wave climate for determining the baseline stress levels on a coastline.

Wave data from hindcast wave models provides coverage in both space and time for long-term wave climate studies, while in situ wave data from moored buoys are often lacking due to the cost of long-term deployment and maintenance. As a result, previous studies have investigated global and local wave power using wave hindcast model outputs (Furuichi et al., 2008; Dobrynin et al., 2012; Soares et al., 2014; Reguero et al., 2015, 2019; Kamranzad et al., 2016; Mentaschi et al., 2017; Ulazia, et al., 2017; Mudelsee, 2019; Ahn and Neary, 2020). Few studies have strictly used moored buoy observation data to calculate wave power to investigate trends, due to the lack of consistent data over time (e.g. Saha et al., 2010; Reguero et al., 2019), as well as instrumentation and processing discontinuity uncertainties within observation time series data (e.g., Gemmrich et al., 2011; Young et al., 2011; Livermont et al., 2015, 2017; and Young and Ribal 2019).

Recently the United States Army Corps of Engineers (USACE) developed a self-describing Quality Controlled and Consistent (QCC) Measurement Archive (Hall and Jensen 2022) that collates historical moored buoy measurements from online NOAA National Data Buoy Center sources, removes data points from periods when the buoys were adrift or undergoing maintenance and verifies all available metadata from in-house NDBC sources for each historical data point. As this study uses these geographically cleaned data and verified metadata from the newly developed USACE QCC Measurement Archive (Hall and Jensen 2022), it confidently identifies instrumentation and system changes that occurred throughout the history of NDBC study sites. These verified metadata enable this study to be the first to offer a viable methodology to remove the observational time series data discontinuations that were highlighted by previous studies (Gemmrich et al., 2011; Young et al., 2011; Livermont et al., 2015, 2017; and Young and Ribal, 2019). Additionally, this study tests for historical shifting trends in wave power using measurement data that are interpolated for missing values and detrended for seasonality, allowing for a continuous time series of moored buoy data with no gaps and or background seasonality variance bias.

As USACE now has two unique wave data resources, the USACE QCC Measurement Archive and a long-term Wave Information Study (WIS) model hindcasts, these resources

enable this unique wave climate study that uses wave data from both model and moored buoys for wave power trend validation and comparisons. Hence, this work compares long-term in situ wave power time series trends and calculations with collocated and concurrent wave model estimates of wave power, allowing for (1) the examination of long-term trends of in situ wave power time series of wave buoy data and (2) the validation of spatially and temporally comparable WIS model estimates.

The paper is organised as follows. Section 2 describes the data used within this work and provides a method for handling in situ observational calculations and discontinuities, before removing seasonality from data signals and outlining definitive statistical analyses. In Section 3.1, evaluations of the collated and concurrent observational and model wave power trends and estimates are discussed, with an overall summary in Section 5..

2 Data and methodology

This work uses the National Oceanic and Atmospheric Administration (NOAA) National Data Buoy Center (NDBC) wave data as they provide one of the longest time series of observational wave data that currently exists. Over the decades, NDBC have developed and refined new moored buoy platforms, sensors, processing protocols and modelling algorithms to improve quality in their wave measurements while responding to increasing demands for providing long-term, high-quality, continuous observational data (Earle et al., 1984, 1999; Steele et al., 1985, 1992; NDBC, 2003; Riley et al., 2011; Riley and Bouchard, 2015). However, these data are known to contain discontinuities within the long time series data, which many have identified and attempted to correct (e.g. Gemmrich et al., 2011; Young et al., 2011; Livermont et al., 2015, 2017; Young and Ribal, 2019; Hall and Jensen, 2021). This work offers a definitive solution to mitigate these discontinuities and develops the first set of wave power values that are calculated from the most accurate NDBC data to date: the newly developed USACE Quality Controlled Consistent Measurement Archive (Hall and Jensen 2022).

Wave power estimates from collated and concurrent USACE WIS datasets are used for comparative trend purposes to evaluate methodologies used within this work. The NOAA National Hurricane Center storm records and three NOAA teleconnection climate indices are included to provide context during interpretation of the observed moored buoy wave power trends.

Review sites are chosen to include a wide variety of wave environments (Fig. 1). West coast and open ocean swell wave environments with large fetch potentials are represented by the eastern Pacific Ocean and Hawaiian time series
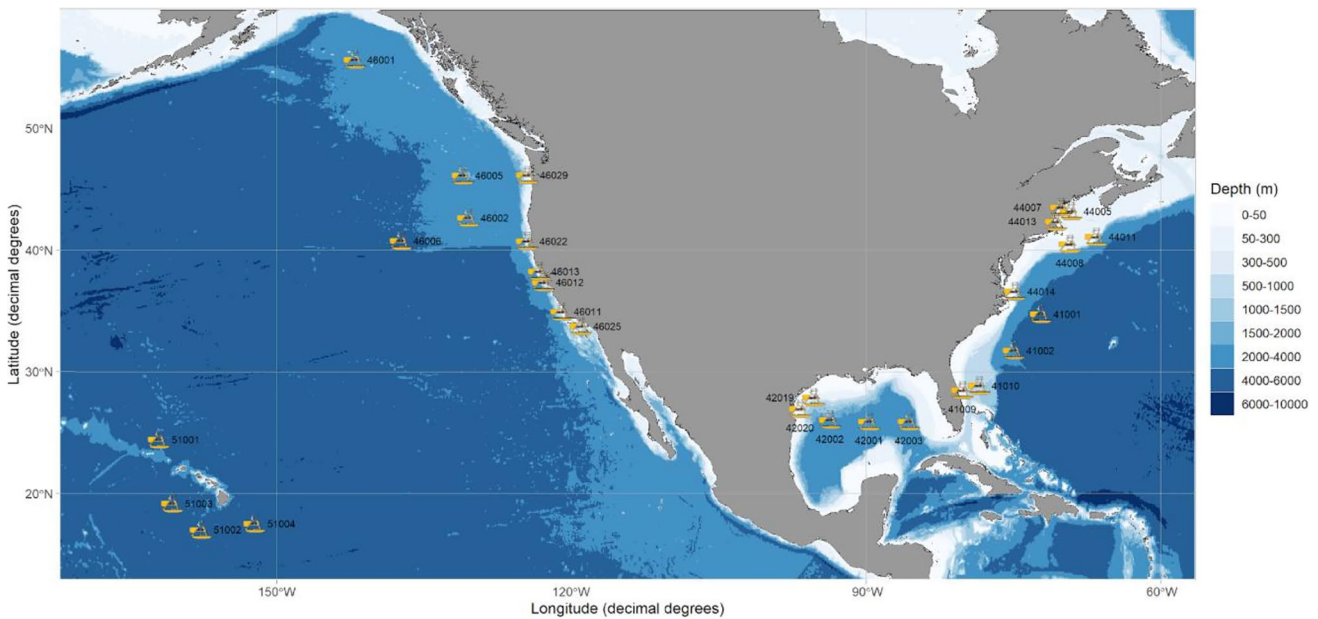
Fig. 1 NDBC and WIS study sites

data. Locally generated wind sea conditions with localised extreme events are showcased by the Atlantic Ocean and Gulf of Mexico data. Great Lakes data that would represent locally generated wind sea conditions are ignored due to the short, summer season deployment periods of these ice-prone winter regions, which are thus riddled with large gaps in the winter wave records that cannot be supplemented. Sites were selected with deployment lengths of 30 years or longer, and deployment locations in waters that are deep enough to negate possible shallow water shoaling effects on wave power estimates. Appendix A details the reviewed NDBC and WIS sites, including their water depths and lengths of record.

All data manipulation and analyses were performed using R software (R Core Team, 2021; RStudio Team, 2021).

2.1 Calculating wave parameters

2.1.1 Wave power calculations

As per Resio et al. (2003), wave power (wave energy flux per metre of wave-crest length in kW/m) is calculated from H_{m0} (m) and T_p (s) as $P \approx \frac{\rho g^2}{64\pi} H_{m0}^2 T_p$, where '$\rho$ is the density of water (998 kg/m^3) and g is the acceleration of gravity (9.81 m/s^2)' (Resio et al., 2003) for deep water waves (where water depth is greater than half the wavelength). The Resio et al. (2003) defined fresh water density constant was retained within this work due to the unavailability of the precise estimate of sea water density at each buoy location through specific regions, years and seasons. Therefore, maintaining this Resio et al. (2003) constant across all stations negates

the regionally variable effects of sea water density within this work. After validation, the *wave_energy* function in the R software *waver* package (Marchand and Gill, 2018), which uses the Resio et al. (2003) equation, is used to calculate wave power.

These wave power calculations require H_{m0} and T_p from the NDBC and WIS datasets. However, prior to those calculations, the NDBC moored buoy data are prepared as follows.

2.1.2 Moored NDBC buoy data

Moored buoy data were collated from the USACE QQC Measurement Archive (Hall and Jensen 2022), stored on the USACE CHL Thredds Server (USACE ERDC, 2022). Multiple works have comprehensively described NDBC's collection methodology, applied calibration techniques and processing protocols for non-directional and directional wave measurements (e.g. Earle et al., 1984, 1999; Steele et al., 1985, 1992; NDBC, 2003; Riley et al., 2011; Riley and Bouchard, 2015). Although NDBC has predominantly used the same wave parameter definitions and equations throughout its history, shore side quality control procedures and collection platforms have advanced through the decades. For example, NDBC has historically used different wave instrumentation (detailed within Appendix B) that record spectral wave energy estimates across two frequency band ranges (NDBC 2003), a 38-band wave spectrum (0.300–0.400 Hz) and a 47-band wave spectrum (0.002–0.485 Hz). The bandwidth is a constant 0.01 Hz for the 38-band wave spectrum. However, the bandwidths of the 47-band wave spectrum are

0.005 Hz, 0.01 Hz and 0.02 Hz for low-, middle- and high-frequency regions, respectively (detailed within Appendix B, NDBC 2003, 2018a; Teng et al. 2009).

With the increase in range and bandwidth variations of the now standard 47-band wave spectrum in the 2000s (instrumentation replacement times differ across NDBC stations due to the variable maintenance schedules), the wave energy is displayed in different frequency bands between older systems and newer systems. Therefore, to account for the variations in wave energy distribution across the spectrum that would result from these different frequency ranges, available NDBC data that were collected using the 38-band wave spectrum were interpolated to match the current NDBC standard 47-band wave spectrum (Appendix C), thereby reassigning captured wave energy within comparable frequency bands. This interpolation ensures that all of the following buoy station wave height, periods and power estimates were calculated from evenly distributed wave energy across consistent frequencies throughout the evaluated time periods.

Once these frequencies were interpolated where necessary, bulk wave parameters were calculated from the now consistent NDBC non-directional spectral frequency $S(f)$ [$C11(f)$ in NDBC nomenclature] to mitigate for possible variance from changing shore-side processing protocols. Significant wave heights were calculated as $H_{m0} = 4\sqrt{m_0}$. m_0 is the variance of the wave displacement time series acquired during the wave acquisition period: $m_0 = \sum_{fl}^{fu}(S(f).d(f))$, 'where the summation of spectral density, $S(f)$, is over all frequency bands, from the lowest frequency f_l to the highest frequency, f_u, of the non-directional wave spectrum and $d(f)$ is the bandwidth of each band'; NDBC, 2018b). Dominant wave period, or peak wave period, is defined as $T_p = \frac{1}{f_p}$ (NDBC, 2003), where f_p represents the peak frequency band.

These frequency interpolations and subsequent recalculations of the NDBC bulk parameters identified that one of the culprits that contribute to the often discussed NDBC data discontinues (Gemmrich et al., 2011; Young et al., 2011; Livermont et al., 2015, 2017; Young and Ribal, 2019) is the historical use of these varying wave spectrum ranges. This observation is evident in the NDBC station 41,009 T_p time series data (Fig. 2, top plot), where the switch between 38-band and 47-band wave spectrum usage adds more frequency bands in the low-frequency range of the wave spectrum and thus decreases the variations of T_p on October 4, 2003 (as identified using the USACE QCC Measurement Archive). However, the bottom plot in Fig. 2 visibly shows how the interpolation of the 38-band wave spectrum into 47 frequency bands and recalculation of peak wave period alleviates this impact, removing obvious discontinuities in this NDBC data record.

Another instrumentation change at NDBC station 41009 (Fig. 2) occurred on October 4, 2003: a switch from the Value Engineered Environmental Payload (VEEP) to the Acquisition and Reporting Environmental System (ARES) payload (as identified within the USACE QCC Measurement Archive), lending obscurity to our statement that T_p discontinuities are caused by different wave spectrum usage. Figure 3 showcases an example of NDBC instrumentation shifts that affected the NDBC calculated T_p at station 46029, where variations are evident between the 38-band and 47-band wave spectrum on January 3, 1997; with a random variation in T_p that is not associated with an instrumentation or system change a few months later (possibly a shore-side processing change) and between the VEEP and ARES payload switch on October 21, 2007 (as identified within the USACE QCC Measurement Archive). Figure 3 indicates that the T_p variations shift with the frequency band change in 1997, but not with the earlier switch from the Data Acquisition and Control Telemetry (DACT) payload to the VEEP on September 1, 1996. Therefore this wave spectral frequency correction utilised within this work decreases variations within the peak period, regardless of deployed NDBC instrumentation or applied shore-side processing protocols, successfully removing discontinuities in the NDBC data records used within this work.

Apart from minimal outlier removal, no other quality control of the calculated bulk parameters was necessary, providing the first published methodology to mitigate NDBC discontinuities discussed by others using NDBC data.

Of note is that data gaps (indicated by black crosses within the bottom plots in Figs. 2 and 3) show hourly time periods where no verified spectral wave data were available for recalculation. For these instances of missing hourly spectral data and where the original hourly NDBC datasets did contain bulk parameter values (Hall and Jensen, 2021; Hall and Jensen 2022), the original NDBC bulk parameter values were inserted into the newly calculated datasets to minimise data gaps. In light of the availability of these spectral data, the minimal offsets that were introduced by augmenting the recalculated datasets with these older NDBC data (that were calculated using the 38-band wave spectrum) are deemed acceptable for this work.

2.1.2.1 NDBC buoy data gap interpolation To investigate the temporal behaviour of the wave power at each site, a continuous time series is required for the following seasonal decomposition of wave power estimates, 90th percentile analyses, trend analyses and context comparison with climate indices. However, interpolation across large data gaps causes oversmoothing of the missing data, primarily over

gaps at the start of the datasets. Therefore, NDBC datasets were subset to disregard large gaps from the early years to remove bias from the final interpolations.

Using an interpolation function within the R software package, *oce* (Kelley, 2018; Kelley et al., 2021), the remaining subset of data were interpolated over time to replace missing values. The function interpolates the data using the Barnes algorithm (Koch et al., 1983), which allows for the handling of sparse data periods.

For computational efficiency, the hourly datasets were aggregated to daily mean datasets. Comparisons between the interpolations of hourly versus aggregated daily mean data showed no loss in data integrity, with the aggregated daily means reducing the need for interpolation of the daily values. Aggregation to daily mean values also removes diurnal and possible tidal effects from the datasets. Therefore, aggregated daily mean values are used with confidence within these next analyses.

These interpolations were applied to all NDBC stations, with results for NDBC station 46001 from 1980 to 2021 showcased in Fig. 4, which depicts the mean daily wave power (top plot) and interpolated mean daily wave power (bottom plot) on a logarithmic scale.

Although Fig. 4 shows the equivalency of the interpolated data (bottom plot) with the original data (top plot), in the final time series data only the missing data within the datasets are augmented with the newly interpolated values. This practice allows for the creation of a continuous dataset that retains the integrity of the original data as much as possible. Henceforth, these new NDBC datasets that are recalculated from the consistent NDBC spectral data, and augmented with interpolated values to replace missing data, are referred to as NDBC data. These recalculated and interpolated NDBC H_{m0} and T_p data are used within the wave power calculations.

2.1.3 WIS model estimates

These continuous, consistent observational wave power datasets that are created using this methodology are compared to collocated and concurrent USACE WIS wave estimates. The WIS effort was established to provide long-term wave estimates along all US coasts, including the Great Lakes, to fulfil the USACE coastal zone operations and project maintenance needs that require assessments of localised wave climates (USACE ERDC, 2020). As wave climate information is scarce due to the lack of temporal and spatial point source measurements at coastal USACE locations, the WIS generates 'hindcast wave estimates (height, wave period and direction) and directional spectral estimates for pre-selected output locations' (USACE ERDC, 2020). Many of these sites are intentionally collocated with the NDBC buoy locations for validation of the WIS wave estimates against wave measurements, which forms an essential part in confirming confidence in the model results.

This study inverses this model-measurement relationship by comparing these wave power measurement trends against the collocated and concurrent WIS wave power estimates. These WIS wave power estimates may be used as reference datasets within this work as they are uniformly calculated from WIS wave parameters that are computed using a consistent set of wind fields, modelling technology and general input parameters that are run on a set grid system.

The WIS uses the WAVEWATCH III® (WW3DG, 2019) model for the Pacific and Atlantic Ocean, and the WAM model (Komen et al., 1994) for the Western Alaska region and the Gulf of Mexico (USACE ERDC, 2020). Importantly, the inclusion of these different wave models denotes that a number of different spectral frequency bands (wave model frequency bands are listed in Appendix C) are used within the calculation of wave bulk parameters. As shown in the section above, the calculation of H_{m0} and T_p wave parameters relies heavily on energy distribution across the spectral frequency range. As the frequency ranges differ both between the NDBC and WIS datasets and between the WIS regions, the bulk parameters used in the calculation of wave power differ in value, resulting in an offset between the comparative wave power estimates. Hence, while trends between the WIS and NDBC wave power estimates are expected to mirror each other, the magnitude of the resultant wave power will not. Without recalculating the WIS H_{m0} and T_p wave parameters used in calculations of WIS wave power (beyond the scope of this work), this offset still allows for the use of the WIS estimates as a reference to evaluate the estimated NDBC wave power trends over time.

2.2 Removing seasonal effects

A seasonal component is evident within the estimated wave power across the four regions. Therefore, the data require the removal of the seasonal component to isolate changing trend signals over time. Ultimately, non-detrended and seasonally detrended daily mean wave power (kW/m) results for each region are evaluated within this work to detect changing trends over time and the importance of seasonality to the overall wave climate.

Three seasonal detrending techniques were tested to determine the most appropriate detection of variable seasonality for this application: the classical decompose method (Kendall and Stuart, 1983); a **T**rigonometric seasonality, **B**ox-Cox transformation, **A**RMA errors, **T**rend and **S**easonal components (TBATS) model (De Livera et al., 2011); and a **S**easonal and **T**rend decomposition using **L**oess (STL) method (Cleveland et al., 1990).

The classical *decompose* function from the base R software *stats* package allows for the selection of both additive

and multiplicative decomposition techniques, where additive ($y_t = S_t + T_t + R_t$) and multiplicative ($y_t = S_t \times T_t \times R_t$) decomposition techniques (y_t refers to the data at period t, S_t the seasonal component, T_t is the trend-cycle component and R_t the remainder, Hyndman and Athanasopoulos, 2018) are applied to the data to identify which model best suits the seasonality (day of the week, day of the month, month of the year, season or annual) of the time series data. However, classical decomposition assumes an annually repeated seasonal component and is not robust to short-term deviations from the norm (Hyndman and Athanasopoulos, 2018), which may smooth and hide an increase in storm seasonality or intensity over time. Additionally, classical decomposition does not extend trend analyses to the tails of the datasets.

To account for the complex seasonality that is crucial for these long periods of environmental time series data, an exponential smoothing state space TBATS model (*tbats* function: using day, month and year seasonal parameters) in the *forecast* package (Hyndman et al., 2021) were applied to the time series, as the model allows for seasonality changes over the period of record. Next, a STL method, which uses an additive decomposition technique to address shifts in seasonal components, outliers and change rates that reduce possible model overfitting (Hyndman and Athanasopoulos, 2018) was tested. The R software *forecast* package offers two STL model methods: a user-defined *stl* function, and a more robust *mstl* function (mSTL) that handles multiple seasonality.

To minimise variability in test results, the various decomposition methods were applied to hourly and aggregated daily mean datasets with minimal data gaps and rigorously scrutinised. Figure 5 provides an example (NDBC station 46029) of the wave power trends obtained from the different decomposition methods tested on the hourly data within this work. Of interest is that the classical *decompose* additive and multiplicative techniques returned identical trends (the NDBC and WIS additive decomposition trend lines are hidden below their associated multiplicative decomposition trend lines in Fig. 5). The manual STL model (*stl* function; abbreviated as STL 13 due to the use of a user-defined seasonal window = 13 in Fig. 5) under predicted trends. The mSTL trend models (black and grey in Fig. 5) appear robust enough to capture trend cycles without overfitting the model.

Therefore, the *mstl* (multiple STL) function, which uses Friedman's 'super smoother' algorithm (Friedman, J. H., 1984a, 1984b) to capture the mean, was chosen as the best method to detrend multiple seasonal periods from the data (parameters: seasonal window = 13, trend cycle window = auto) as it allows for a gradual change in possible trend cycles over time without overfitting the model. Additionally, unlike the classical decomposition methods, the mSTL function captured trend estimates across the full tails of the time series.

Of interest is that Fig. 5 clearly depicts the magnitude of the offsets between the NDBC and WIS wave power estimates as expected from the use of the non-uniform NDBC and WIS spectral ranges for bulk parameter calculations. However, the WIS and NDBC decomposition trends are in agreement within Fig. 5, as within all of the reviewed sites, definitively highlighting the accuracy of the measurement methodology used within this work, as well as the use of WIS as a stable reference for wave climate analyses.

A second methodology check that relied on these trend analyses was an evaluation of the possible loss of data integrity during aggregation of the hourly data into daily mean datasets. A review of the NDBC and WIS hourly vs aggregated daily mean decomposition trends showed no loss of data integrity. However, of interest is that the daily mean trends align more consistently with temporal-associated climate index regression trends than the hourly data, allowing for extra confidence in utilising these aggregated daily mean datasets for these wave power trend analyses.

2.3 Climate indices

In an effort to interpret the peaks and troughs in the general wave power trends observed within this work, teleconnection climate indices are incorporated for the Pacific and Atlantic Ocean regions. Trends in these climate indices provide context as to whether the wave power trends echo these climate trends after the removal of seasonal effects, or whether the wave power trends are only directly related to wind-driven storm events. Three climate indices are reviewed: the El Niño/Southern Oscillation (ENSO), a periodic fluctuation in sea surface temperature and air pressure that affects global weather (PSL, 2021; NCEI, 2021a), and two basin-specific indices: the longer-lived Pacific Decadal Oscillation (PDO) Index that affects the Pacific Basin ocean temperatures and sea-level pressures (NCEI, 2021b), and the North Atlantic Oscillation (NAO) index of sea-level pressure, which affects the intensity and location of storm tracks and the North Atlantic jet stream, and is 'based on the surface sea-level pressure difference between the Subtropical (Azores) High and the Subpolar Low' (NCEI, 2021c).

Odérix et al. (2020) reviewed four ENSO products and determined that the Multivariate ENSO Index Version 2 (MEI.v2) index is the product of choice to investigate global wave power. The MEI indices, which represent both oceanic and atmospheric variables, were sourced from the NOAA Physical Sciences Laboratory (https://www.psl.noaa.gov/enso/mei, downloaded on December 29, 2021). The PDO indices (Mantua, 2002) were sourced from the NCEI PDO database (NCEI, 2021b) and are based on NOAA's extended reconstruction of SSTs (ERSST Version 5). The NAO indices were also sourced from the NCEI NAO database (NCEI, 2021c) and are based on the 'NAO loading pattern to the

daily anomaly 500 millibar height field over 0–90°N' (NCEI, 2021c).

2.4 Statistical evaluations

The following goodness of fit statistical analyses tested the relationship amongst and between the various moored buoy test sites and the WIS model data estimations. Relationships between the co-located NDBC and WIS are assessed by Pearson correlation coefficients ($r = \frac{\sum xy}{\sqrt{\sum x^2 \sum y^2}}$; Zar, 1984), with coefficients = 1 implying a perfect fit.

Linear regressions evaluate the trends of the datasets ($Y_i = a + bX_i$, with X representing the independent variable, Y the dependent variable, a the intercept and b the slope; Zar, 1984). The curve of the data are showcased by locally weighted scatterplot smoothing (LOWESS) regressions as $(\sum_k w(x_k)G(x_k)(y_k - a - bx_k)^2$ for $k = 1,...,N$, with a calculation of the robust weighting functions, $w(x_k)G(x_k)$ and regression smoothing, $y_k - a - bx_k$, for each data point (Cleveland, 1979).

Descriptive statistics (Zar, 1984) mean [$\overline{X} = \frac{\sum x}{n}$, where n is the size of the sample x], median [$Med(X) = X_{(n+1)/2}$, if n is odd; $Med(X) = \frac{X_2 + X_{(n/2)+1}}{2}$ if n is even], 90th and 99th percentile [$X = \overline{X} + Z\sigma$, where σ represents the standard deviation and $Z = 1.282$ for the 90th quantile and 2.326 for the 99th quantile] are used to investigate wave power intensity at each site over the reviewed time period. The standard error is computed as $SE = \frac{\sigma}{\sqrt{n}}$ (Zar, 1984).

3 Trends in wave power

3.1 Regional correlations between NDBC and WIS wave power estimates

Correlations between the NDBC and WIS wave power estimates test the concurrent and collated use of these datasets for comparative wave power trend analyses. Figure 6 shows the Pearson correlation coefficients (r) of the NDBC and WIS seasonally detrended, daily mean wave power estimates for all sites across the reviewed regions. As expected, correlation coefficients (0.95, 0.78, 0.92 and 0.93 for daily mean wave power for the eastern Pacific Ocean, Hawaiian Island, Gulf of Mexico and Atlantic Ocean sites respectively) between the NDBC and WIS data show good agreement for all regions apart from the Hawaiian sites (Fig. 6).

This drop in correlation agreement within the Hawaiian sites is due to the lower efficiency of WIS to predict low wave conditions within the trade winds (Jensen, 2022, pers. comms., USACE WIS Principle Investigator). This is because WIS estimates wave conditions from large mesoscale wind conditions within that region, while Hawaii

wave conditions are driven by localised weather systems that affect model estimates (Stopa et al., 2011; Li et al., 2021). During mixed wind seas and swells, WIS tends to select the swell system over the wind seas, resulting in an overestimation of the wave power estimates compared to the measurements (Jensen, 2022, pers. comms.). Additionally, these Hawaii results only represent two buoy sites (northwest and south of the Hawaiian Islands, which in the latter case is in a sheltered region), reducing any normalisation that would be introduced by additional locations; in essence, amplifying the variability signal observed at only these two specific sites. Overall, comparisons between the NDBC and WIS data at the Hawaii sites still reflect the overestimation trends observed within the eastern Pacific Ocean data comparisons, just to a greater degree.

Another heterogeneity component between the two data sources may be the coupling effects of wave-current interaction that are reported in NDBC wave measurements (Wang et al., 1994; Steele, 1997). NDBC does not rectify the net effects of surface currents within wave measurements, while WIS estimates do not contain a current component, adding to the variance between the two datasets. However, these current interactions are beyond the scope of this work and are therefore disregarded within these comparisons.

Overall, the largest daily mean wave power values were calculated for the eastern Pacific Ocean and the Hawaiian sites. Lower daily mean wave power values register at the Atlantic Ocean sites, with the lowest daily mean wave power values estimated for the Gulf of Mexico region (Fig. 6). The Atlantic Ocean WIS sites underestimate wave power when compared to collocated and concurrent NDBC wave power values, while WIS appears to be overestimating wave power within the eastern Pacific Ocean, Gulf of Mexico sites, and as expected, within the Hawaiian sites (Fig. 6). However, even with these over- and underestimates of wave power across the reviewed regions, the offsets between the NDBC and WIS decomposition trends still appear constant over time for each site (Fig. 5).

3.2 Eastern Pacific Ocean wave power

Data collected at ten eastern Pacific Ocean NDBC moored buoy sites shows maximum hourly (with seasonal effects included) intra-site wave power ranges between 416.16 kW/m (number of observations [n] = 12,766) at NDBC 46025 to 1249.94 kW/m (n = 10,307) at NDBC station 46022 (Table 2). The maximum hourly wave power at NDBC station 46025 is consistent with the expected lower wave power within the Southern California Bight, which is sheltered from North Pacific storms events, and the Channel Islands, which are not directly exposed to South Pacific and Southern Ocean swell events (Fig. 1, NDBC 46025). In contrast, a high maximum hourly wave power at NDBC

Table 1 Eastern Pacific Ocean hourly wave power (kW/m) descriptive statistics for each site (displayed from North to South) for the reviewed 40-year period

Station	Median	Mean	90th percentile	99th percentile	Max.	Number of Obs.	Std. deviation	Std. error
NDBC 46001	25.47	48.29	117.14	307.12	893.12	13,920	63.96	0.54
WIS 46001	25.93	52.41	131.27	357.38	961.37	13,346	72.19	0.62
NDBC 46005	27.79	54.22	131.04	353.56	1135.07	12,253	74.07	0.67
WIS 46005	34.97	68.79	169.15	426.77	1153.04	11,322	90.34	0.85
NDBC 46029	19.05	38.41	93.48	273.02	651.12	8939	53.34	0.56
WIS 46029	23.03	46.00	110.64	315.02	894.02	8612	61.91	0.67
NDBC 46002	27.51	51.41	121.84	341.47	1067.81	11,263	68.68	0.65
WIS 46002	34.05	64.90	157.53	408.10	1772.31	10,931	86.08	0.82
NDBC 46006	30.89	60.84	147.65	406.40	1206.18	9821	83.07	0.84
WIS 46006	38.03	74.14	180.72	479.54	1562.52	9516	99.76	1.02
NDBC 46022	24.31	40.98	94.32	253.76	1249.94	10,307	52.22	0.51
WIS 46022	31.51	51.66	117.06	296.59	789.64	9781	59.30	0.60
NDBC 46013	20.00	32.29	72.17	171.97	674.46	12,446	37.02	0.33
WIS 46013	24.29	39.87	89.28	215.97	595.46	12,073	44.40	0.40
NDBC 46012	18.89	30.33	68.30	168.19	611.87	11,681	34.60	0.32
WIS 46012	22.95	36.06	79.13	186.07	604.47	11,109	38.71	0.37
NDBC 46011	17.61	28.37	62.71	162.93	602.95	12,449	33.54	0.30
WIS 46011	22.79	37.34	83.90	209.78	601.29	11,875	42.62	0.39
NDBC 46025	5.56	8.21	15.63	46.98	416.16	12,766	10.48	0.09
WIS 46025	4.51	7.59	15.06	52.76	381.65	12,226	11.88	0.11

station 46022 is observed in the open waters offshore of Eel River near Eureka, California (NDBC 46022).

Moored buoys are notorious for breaking adrift from their moorings during extreme weather events, compromising any wave data collected while untethered from the sea floor (Eulerian moored buoy data processing algorithms are not designed for Lagrangian movement). Therefore, of particular interest is the loss of viable maximum wave heights and periods (the building blocks of wave power) that may be recorded during these storm events. Hence, in the absence of true maximums, 90th and 99th percentile wave power values provide a more reliable comparison of wave power intensity across the individual stations. Within the reviewed eastern Pacific Ocean buoy sites (Table 1), NDBC station 46006 is subjected to the highest 90th and 99th percentile wave power due to its exposed, offshore, open ocean position.

A review of the suspect maximum recorded values and more reliable 90th and 99th percentiles across the individual eastern Pacific Ocean stations (Table 2) highlights a significant increase in wave power intensity caused by a few passing storm events. Similar wave power differences are evident in the variance between the median and mean values across the individual stations (Table 2), highlighting that the majority (median) of the wave power occurring at each site is lower than the mean. This again showcases the effects of storm events with standard deviations that are higher than both the median and mean wave power estimates. For example, NDBC station 46001 experienced mean hourly wave power of 48.29 kW/m across its lifetime, with a higher standard deviation of 63.96 kW/m, while the median wave power values at that site were far less at 25.47 kW/m (Table 2). These results indicate that the wave power distribution is highly skewed by a few intense storms. Standard errors across the datasets remain low overall (Table 2), allowing for confidence in the estimated wave power values.

Of note is that Table 2 clearly highlights the offset between the WIS and NDBC hourly wave power estimates, where 99th percentile WIS wave power estimates are consistently higher for all of the sites. The maximum wave power is only higher for the WIS sites across the northern sites (stations 46001–46006). This pattern reverses for the southern sites (stations 46022–46025), where maximum wave power is consistently lower than the NDBC estimates (Table 2).

After removal of seasonal effects, NDBC daily mean wave power trends within the eastern Pacific Ocean show agreement across the sites, with the majority of the sites remaining with 20–82 kW/m (Fig. 7), and only NDBC station 46025 returning a mean daily wave power trend that oscillates around 10 kW/m (Fig. 7). Four significant peaks in 1997, 2006, 2015 and 2016 reflect the large number of tropical cyclones and depressions (19, 21, 22 and 22 storms

Fig. 2 Published NDBC hourly T_p (top) vs calculated hourly NDBC T_p (bottom) over time for NDBC station 41009, with orange boxes highlighting variations in peak period. Colours represent deployed hull types. Historical timelines highlighting the use of verified payload type (payload acronyms are described in Appendix B) and frequency bands are shown for NDBC station 41009. Mooring type and depth were constant for the full station deployment history. Black crosses indicate where original, hourly NDBC data are available to augment missing data within the recalculated dataset
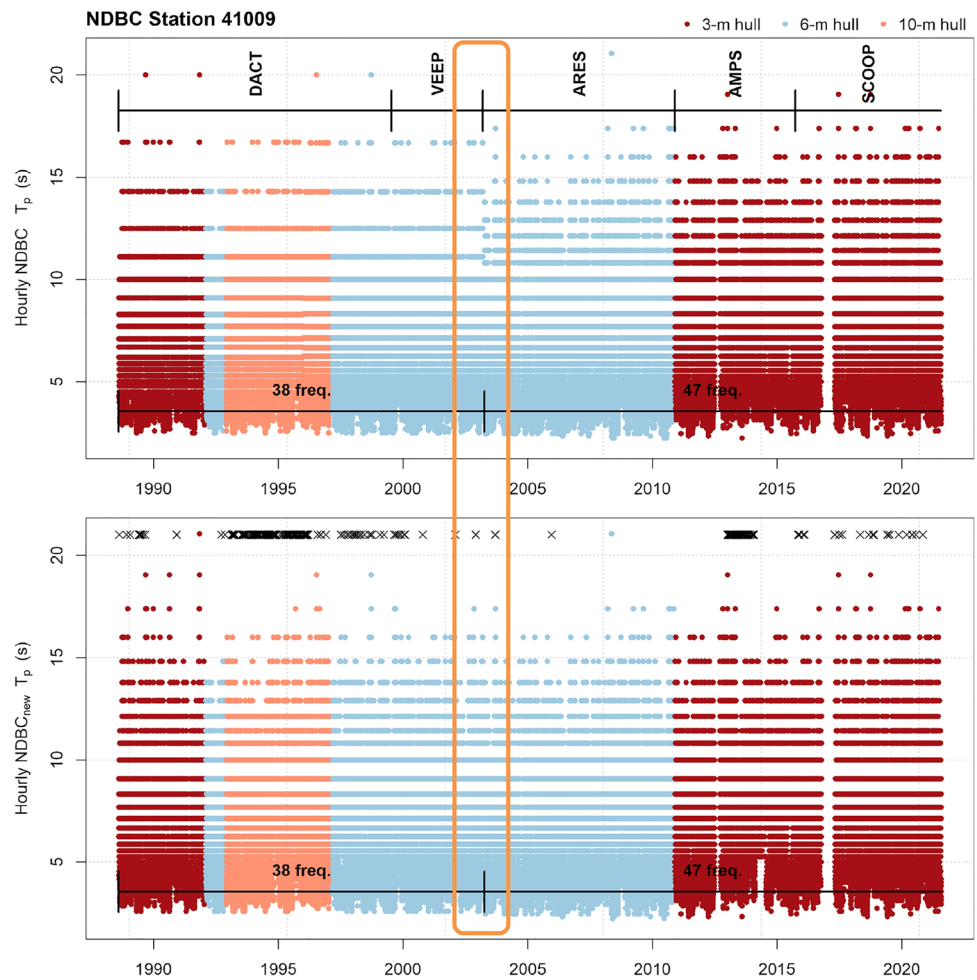
in those years respectively: Appendix D), as recorded by the NOAA National Hurricane Center (NHC) for 1995–2021 (NHC, 2022).

Peaks in these linear regression trends appear to follow trends in both PDO and ENSO LOWESS regressions (Fig. 7), where the peaks in wave power that are evident in 1987 are associated with both the PDO and ENSO peaks. However, the ENSO peak in 1992 appears aligned with the wave power peaks observed in NDBC stations 46012 and 46013, while the wave power peaks at NDBC stations 46005 and 46002 match the PDO peak in 1993 (Fig. 7). Similar differences are observed within the 1982–1984 years, where NDBC stations 46011 and 46012 wave power trends appear to peak in time with the ENSO index, while NDBC stations 46013 and 46005 wave power trends align with the peak in the PDO index. Therefore both of these climate indices provide valuable context to the observed eastern Pacific Ocean wave power trends, especially in the absence of NHC storm counts for these earlier years.

As expected, linear regression trends vary across the spectrum of eastern Pacific Ocean NDBC sites (Fig. 7) as each site experiences different environmental forcing.

NDBC station 46022 shows the greatest (downward) wave power trend across the stations (Table 4), which is expected as that site also exhibits the maximum wave power (Table 2).

Of note is the difference in statistical significance between the collocated and concurrent NDBC and WIS wave power trends for the reviewed sites. All but three sites (70%) show statistically significant trends (p-value less than 0.05) across the eastern Pacific Ocean NDBC stations for both the non-detrended and seasonally detrended daily mean wave power, while all WIS sites estimated significant trends (Table 2). However, all sites exhibited an acceptable NDBC-WIS Pearson correlation coefficient of 0.87 or higher (Table 2).

The relative agreement between the overall trends between each site's wave power estimates that include seasonality (Table 4: wave power trends per year), wave power estimates that are seasonally detrended (Table 4: seasonally detrended wave power trends per year) and the associated daily slopes and intercepts suggests that within the eastern Pacific Ocean sites, statistical trend significance appears independent of seasonal effects. All trends per year are downward, apart from site 46012 (Table 4), which is offshore of Half Moon Bay, near San Francisco, CA (Fig. 1).

Fig. 3 Published NDBC hourly T_p (top) vs calculated hourly NDBC T_p (bottom) over time for NDBC station 46029, with orange boxes highlighting variations in peak period. Colours represent deployed hull types. Timelines highlighting the usage of verified payload type (payload acronyms are described in Appendix B), mooring and frequency bands are shown for NDBC station 46029. Black crosses indicate where original, hourly NDBC data are available to augment missing data within the recalculated dataset
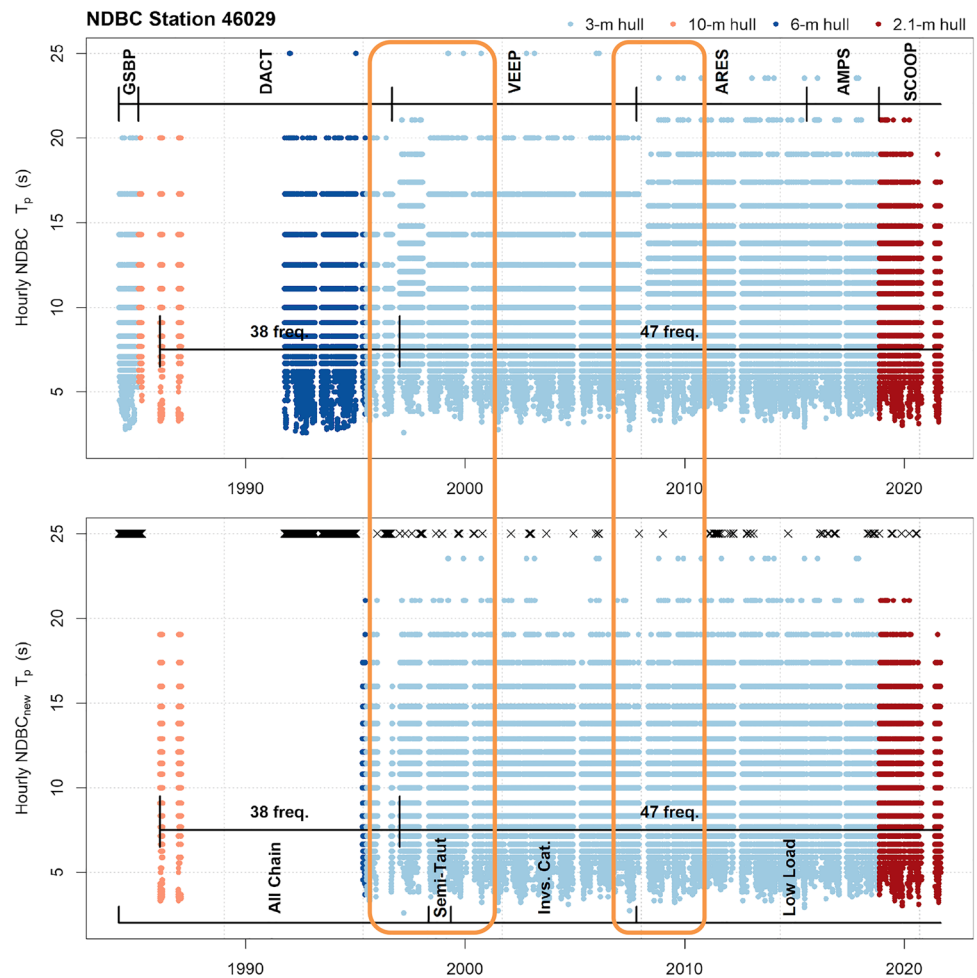
Intriguingly, site 46013 (Fig. 1), which is just up the coast to site 46012, shows a downward trend. A trend difference of 0.098 kW/m/year separates the two NDBC stations (Table 4), even though both of these coastal shelf stations experience similar wave conditions that have developed over large distances. Overall, while seasonal detrending does not appear to affect overall statistical significance in wave power trends within the eastern Pacific Ocean, the annual wave power per year amounts varies, justifying the use of these trend analysis methodologies for coastal planning (Table 4).

In summary, these trend results show agreement with some previous wave trend estimates in slope but are not unanimous in magnitude. For example, Reguero et al. (2015) used the WaveWatchIII model to calculate eastern Pacific Ocean wave power trends of 0.5 kW/m/year (28 years of data), while Wu et al. (2018) projected wave power trends of -0.2 kW/m/year (32 years of data) that are more in agreement with our results. Of note is that these results are estimated across $1.0° \times 1.0°$ and $1.5° \times 1.0°$ resolution eastern Pacific Ocean model grids respectively, so are not comparable in magnitude to the discrete wave power trends per year calculated at each site within this work. Results that are

comparable are the eastern Pacific Ocean buoy results within Ahn and Neary (2020) that show an inter-annual mean total wave power of -0.13 kW/m/year (30 years of data) for NDBC buoy 46026, which, possibly due to the use of different wave power calculations, is only comparable in slope to the nearby NDBC buoy 46012 (0.20 and 0.21 kW/m/year for the non-detrended and seasonally detrended wave power respectively) reviewed within this work (Table 2). Interestingly, Ahn and Neary (2020) results are more closely aligned with the magnitude of the WIS wave power results of 0.11 and 0.12 kW/m/year for the non-detrended and seasonally detrended data respectively, although trend slopes still differ (Table 2).

3.3 Hawaii wave power

Travelling westwards into the open Pacific Ocean waters, Table 3 describes the wave power environment at the Hawaiian island review sites. Only four sites around the Hawaiian Island chain met the study parameters of deployment lengths of 30 years or longer. Additionally, NDBC stations 51003
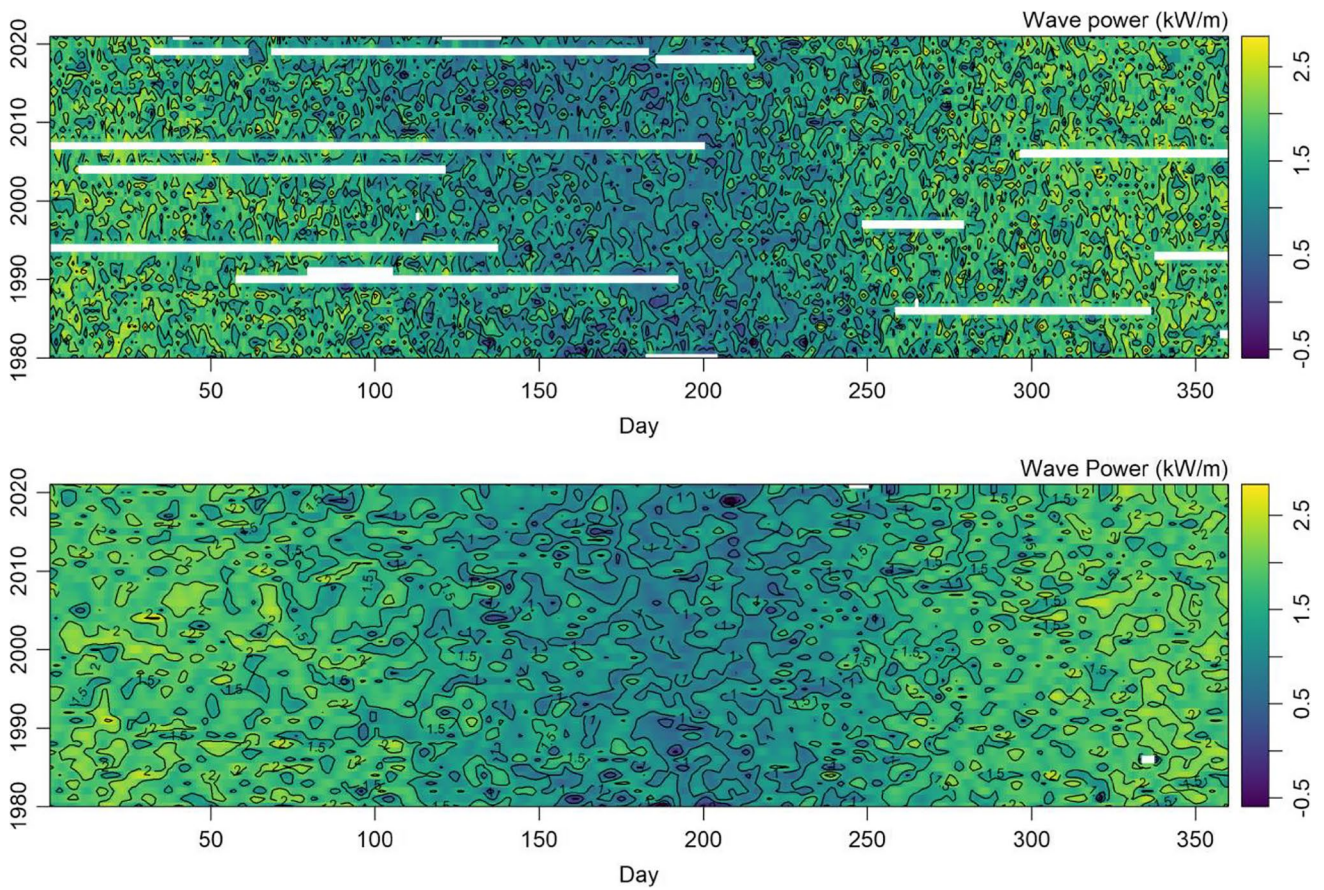
Fig. 4 Heatmaps of mean daily wave power (top) and interpolated mean daily wave power (both in kW/m and on a $\log_{10}$ scale) for NDBC station 46001 from 1980 to 2021
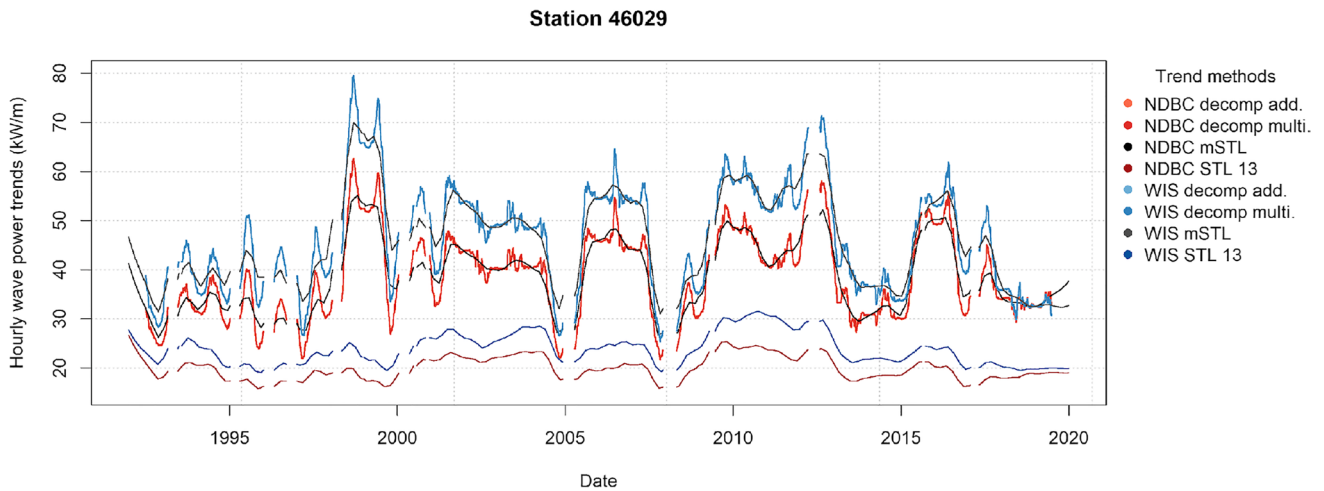
Fig. 5 Decomposition methods for hourly wave power time series for NDBC station 46029

and 51004 do not have corresponding WIS grid points for reference.

The reviewed Hawaiian Island sites show the same maximum versus 90th and 99th percentile variability in wave power intensity (Table 3) that was observed within the eastern Pacific Ocean sites. WIS site 51001 shows an exorbitant maximum of 2212.66 kW/m ($n = 8944$), which does not correspond to the maximum wave power of 706.59 kW/m

Fig. 6 Scatter diagrams depicting the correlations between the NDBC vs WIS seasonally detrended, daily mean wave power (kW/m) for each region. Dashed red lines indicate linear regressions, with sample size and Pearson correlation coefficients (*r*) listed in the top right corner. All plots include a dotted grey 1–1 line for reference
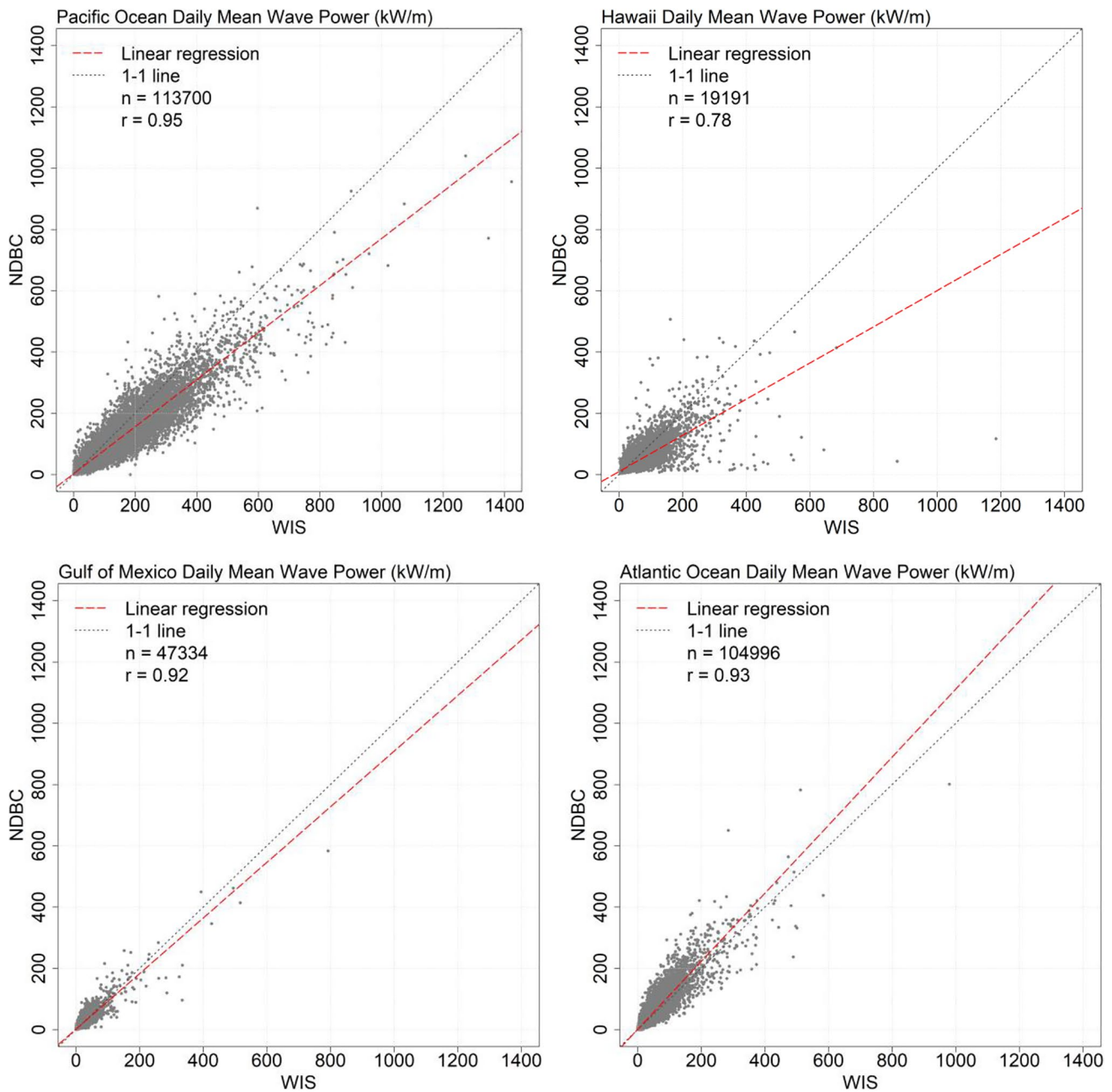
($n = 9488$) that is identified at the collocated and concurrent NDBC station 51001 (Table 3).

NDBC station 51001 (Fig. 1) shows significantly higher values for 90–99th percentile and maximum wave power than the other Hawaiian sites, highlighting its unique location to the north of the Hawaiian Island chain with exposure to north Pacific storm swells. The rest of the reviewed Hawaiian sites fall within the southern lee of the island chains, receiving wave signals from swells originating from distant Southern Ocean storms. Again storm swell effects are evident in the standard deviations for each site across the 36-year review timeframe, with NDBC station 51001 showing a standard deviation (43.34 kW/m) of approximately twice its median wave power estimate (22.99 kW/m; Table 3). This pattern is far less evident in the southern sites, with median and standard deviations that are within relative agreement (Table 3). Again, standard errors remain low across the reviewed sites (Table 3).
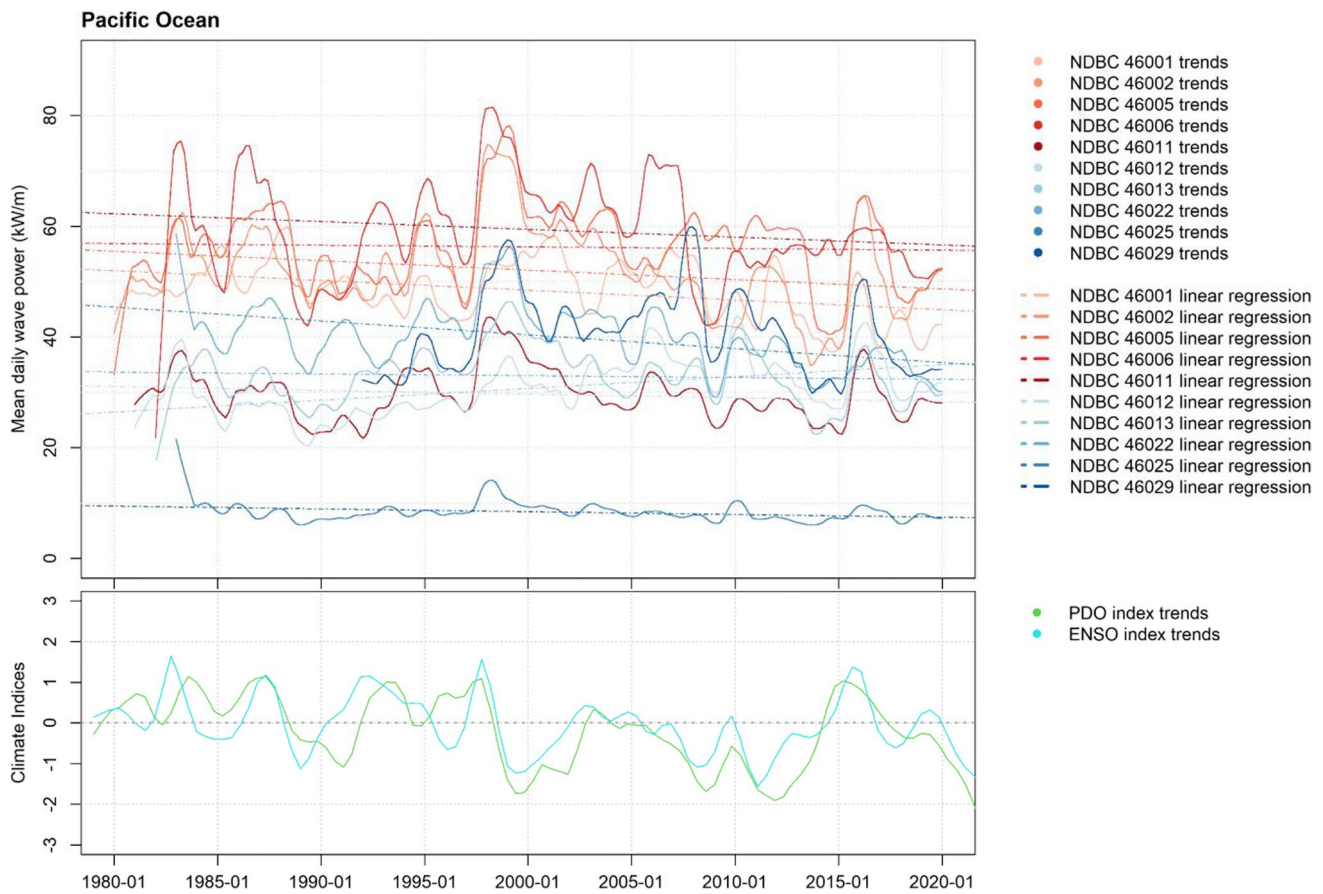
Fig. 7 NDBC wave power trends and overall linear regressions for the eastern Pacific Ocean (top plot), with concurrent LOWESS regressions of the reference PDO and ENSO indices for trend context (bottom plot)

This offset in northern versus southern wave values are echoed within the overall trends of the time series data (Fig. 8), where mean daily wave power for NDBC station 51001 registers higher (30–50 kW/m) than the rest of the Hawaiian sites (20–40 kW/m). The peak in mean daily wave power during 1997 (Fig. 8) mirrors the nine tropical cyclones and depressions that were recorded by the NHC within the Central Pacific Ocean during that year (Appendix D). Similarly, the 2015 peak in wave power reflects the five tropical cyclones and depressions listed by the NHC (Appendix D) for the region. Again, trends in the wave power (kW/m) show a temporal agreement with the PDO and ENSO LOWESS regression trends, where both climate trends match peaks in NDBC 51002 and 51003 wave power in 1987, and again in 1997 and 2010 (Fig. 8). The peaks in the PDO index appear reflected within the 1993 peaks in wave power at NDBC station 51004, and the 2001 peaks across all of the reviewed NDBC sites (Fig. 8). A smaller peak in 2012 is evident in wave power at NDBC station 51004 that coincides with a peak in the ENSO index (Fig. 8), justifying the use of both climate indices to provide context to the Hawaiian Island sites.

The disagreement in NDBC and WIS wave trends for site 51001 are clearly evident in the low 0.78 and 0.67 Pearson correlation coefficients for non-detrended and seasonally detrended data respectively (Table 4). These results show that all trends, both non-detrended and seasonally detrended data, are downward at the Hawaiian sites (Table 4), indicating that wave power has decreased slightly over the reviewed 36-year time period. Again, trend statistical significance (p-value less than 0.05) appears independent of seasonal effects, with 100% of the reviewed sites showing a downward trend in wave power over the 36-year time period (Table 4). These results agree in slope but are not comparable in magnitude (with -1.16 and -1.15 kW/m/year for non-detrended and seasonally detrended wave power) with Ahn and Neary's (2020) recent 30-year review, which estimated an inter-annual mean total wave power of -0.25 kW/m/year for NDBC station 51001.

3.4 Atlantic Ocean wave power

Results show less wave power within the Atlantic Ocean than in the eastern Pacific Ocean, with a maximum hourly

Table 2 Eastern Pacific Ocean 40-year regression trends for each site (displayed from North to South) for non-detrended and seasonally detrended daily mean wave power (kW/m). Significant trends per year are indicated in bold (*p*-value < 0.05)

Station	Wave power trends (kW/m/yr.)	Wave power slope (kW/m/day)	Wave Power intercept (kW/m)	NDBC/WIS Pearson correlation coefficient	Seasonally detrended wave power trends (kW/m/yr.)	Seasonally detrended wave power slope (kW/m/day)	Seasonally detrended wave power intercept (kW/m)	Seasonally detrended NDBC/WIS Pearson correlation coefficient	Number of samples
NDBC 46001	**− 0.173**	− 0.00047	53.715	0.93	**− 0.176**	− 0.00048	53.721	0.91	14,611
WIS 46001	**− 0.105**	− 0.00029	55.288		**− 0.107**	− 0.00029	55.264		
NDBC 46005	− 0.036	− 0.00010	57.391	0.95	− 0.029	− 0.00008	57.200	0.93	14,611
WIS 46005	**− 0.117**	− 0.00032	74.518		**− 0.107**	− 0.00029	74.230		
NDBC 46029	− 0.071	− 0.00019	43.374	0.91	− 0.069	− 0.00019	43.291	0.87	10,228
WIS 46029	**− 0.221**	− 0.00061	55.934		**− 0.216**	− 0.00059	55.751		
NDBC 46002	**− 0.161**	− 0.00044	57.045	0.95	**− 0.170**	− 0.00047	57.181	0.93	14,285
WIS 46002	**− 0.149**	− 0.00041	70.019		**− 0.161**	− 0.00044	70.198		
NDBC 46006	**− 0.158**	− 0.00043	64.290	0.96	**− 0.140**	− 0.00038	63.646	0.94	13,880
WIS 46006	**− 0.256**	− 0.00070	80.829		**− 0.232**	− 0.00063	79.986		
NDBC 46022	**− 0.255**	− 0.00070	48.108	0.94	**− 0.249**	− 0.00068	47.873	0.91	13,515
WIS 46022	**− 0.292**	− 0.00080	59.778		**− 0.285**	− 0.00078	59.504		
NDBC 46013	− 0.040	− 0.00011	34.207	0.94	− 0.032	− 0.00009	33.975	0.92	13,867
WIS 46013	**− 0.106**	− 0.00029	43.619		**− 0.096**	− 0.00026	43.330		
NDBC 46012	**0.204**	0.00056	24.608	0.93	**0.213**	0.00058	24.326	0.92	14,245
WIS 46012	**0.113**	0.00031	32.338		**0.124**	0.00034	31.944		
NDBC 46011	**− 0.077**	− 0.00021	32.018	0.94	**− 0.067**	− 0.00018	31.706	0.92	14,245
WIS 46011	**− 0.170**	− 0.00047	43.906		**− 0.157**	− 0.00043	43.490		
NDBC 46025	**− 0.055**	− 0.00015	10.125	0.89	**− 0.050**	− 0.00014	9.980	0.88	13,515
WIS 46025	**− 0.064**	− 0.00018	9.782		**− 0.059**	− 0.00016	9.605		

Table 3 Hawaiian Island hourly wave power (kW/m) descriptive statistics for each site (displayed from North to South) for the reviewed 36-year period

Station	Median	Mean	90th percentile	99th percentile	Max.	Number of Obs.	Std. deviation	Std. error
NDBC 51001	22.99	37.09	76.56	224.81	706.59	9488	43.34	0.44
WIS 51001	28.71	47.56	102.29	276.67	2212.66	8944	59.52	0.63
NDBC 51003	20.13	27.26	53.19	119.46	321.38	11,467	23.05	0.22
NDBC 51004	23.97	30.10	55.37	109.81	391.32	9732	22.11	0.22
NDBC 51002	23.38	29.32	53.89	107.37	259.18	10,510	20.84	0.20
WIS 51002	25.76	33.39	63.97	128.59	371.11	9919	25.21	0.25

intra-site wave power range between 384.47 kW/m (*n* = 9453) at NDBC station 44014, to 906.36 kW/m (*n* = 10,132) at NDBC station 41002 (Table 5). NDBC station 44011, which is subjected to frequent

Nor'easter storms, appears the most energetic over the reviewed 40-year period, with 90th and 99th percentile of the waves experienced by that station measuring wave power of 59.01 and 199.88 kW/m.
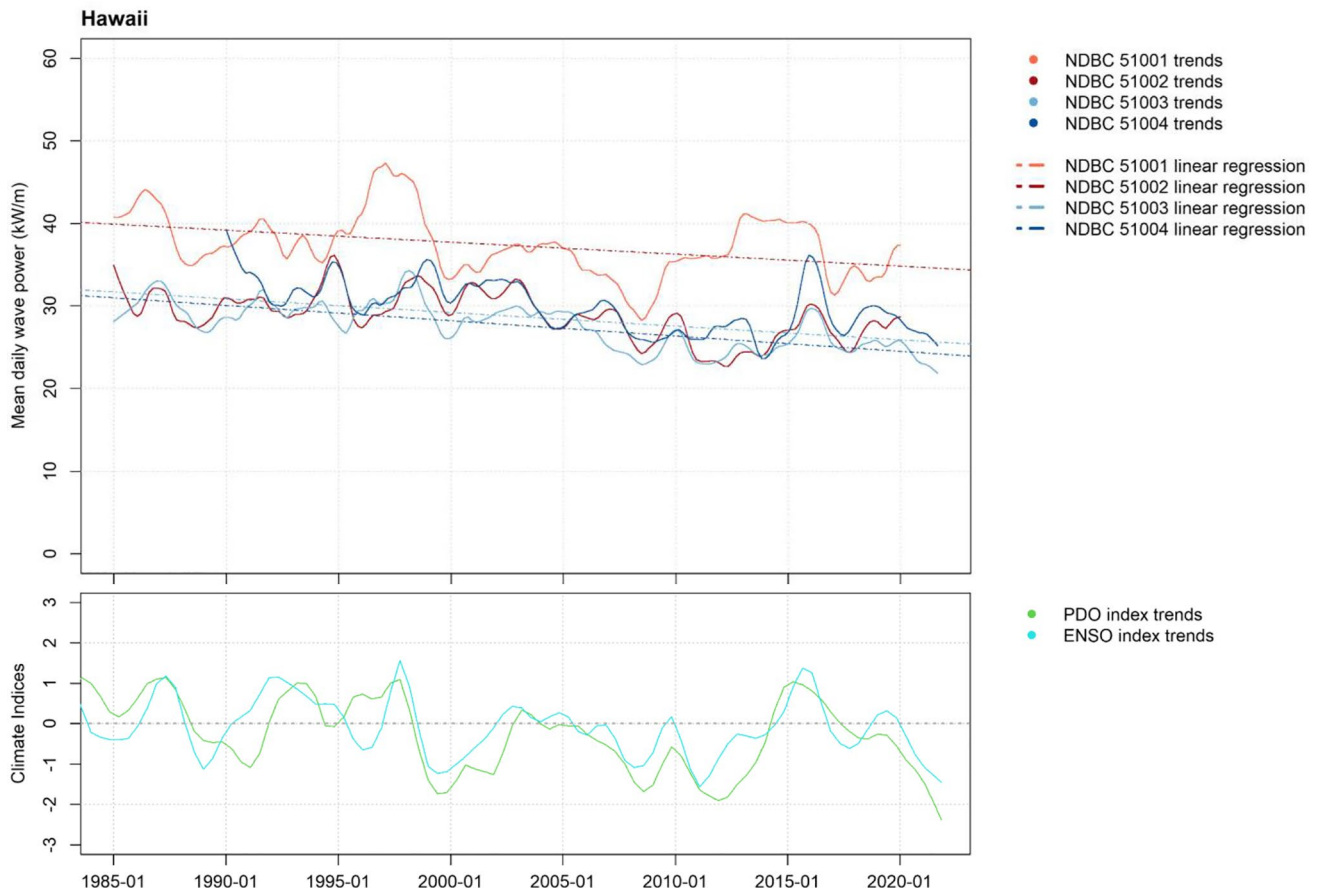
Fig. 8 NDBC wave power trends and overall linear regressions for Hawaii (top plot), with concurrent LOWESS regressions of the reference PDO and ENSO indices for trend context (bottom plot)

Table 4 Hawaiian Island 36-year regression trends for each site (displayed from North to South) for non-detrended and seasonally detrended daily mean wave power (kW/m). Significant trends per year are indicated in bold (p-value < 0.05)

Station	Wave power trends (kW/m/year)	Wave power slope (kW/m/day)	Wave power intercept (kW/m)	NDBC/WIS Pearson correlation coefficient	Seasonally detrended wave power trends (kW/m/year)	Seasonally detrended wave power slope (kW/m/day)	Seasonally detrended wave power intercept (kW/m)	Seasonally detrended NDBC/WIS Pearson correlation coefficient	Number of samples
NDBC 51001	**− 0.163**	− 0.00045	42.647	0.78	**− 0.145**	− 0.00040	42.073	0.67	12,784
WIS 51001	**− 0.495**	− 0.00136	61.867		**− 0.470**	− 0.00129	61.029		
NDBC 51003	**− 0.195**	− 0.00053	34.077	-	**− 0.185**	− 0.00051	33.744	-	13,392
NDBC 51004	**− 0.210**	− 0.00057	37.369	-	**− 0.198**	− 0.00054	36.949	-	11,566
NDBC 51002	**− 0.171**	− 0.00047	34.373	0.83	**− 0.166**	− 0.00045	34.183	0.76	12,784
WIS 51002	**− 0.143**	− 0.00039	37.025		**− 0.132**	− 0.00036	36.664		

Of note is that the mean and median wave power values recorded within the Atlantic Ocean are approximately five times lower than those observed within the eastern Pacific Ocean. These results are due to the difference in storm systems that affect the two areas, as well as the position of the buoys relative to the open ocean within each region, both affecting the T_p values that feed into the wave power estimations.

Table 5 Atlantic Ocean hourly wave power (kW/m) descriptive statistics for each site (displayed from North to South) for the reviewed 40-year period

Station	Median	Mean	90th percentile	99th percentile	Max.	Number of Obs.	Std. deviation	Std. error
NDBC 44007	2.02	5.60	12.18	60.72	414.61	13,015	13.66	0.12
WIS 44007	1.63	3.97	9.16	38.22	161.92	12,410	7.89	0.07
NDBC 44005	4.99	12.79	29.87	117.54	411.43	10,805	24.06	0.23
WIS 44005	3.53	8.49	20.41	74.22	328.98	10,506	15.38	0.15
NDBC 44013	1.34	5.13	10.57	66.97	496.36	10,895	14.94	0.14
WIS 44013	0.93	3.11	6.89	36.40	196.61	10,355	8.12	0.08
NDBC 44011	9.88	24.00	59.01	199.88	751.05	9490	40.54	0.42
WIS 44011	7.75	18.53	44.81	152.90	980.83	9202	34.11	0.36
NDBC 44008	7.34	17.93	43.22	162.33	744.55	11,316	32.59	0.31
WIS 44008	6.22	14.58	35.07	126.79	634.79	10,728	26.63	0.26
NDBC 44014	4.97	11.58	26.58	107.64	384.47	9851	20.99	0.21
WIS 44014	5.09	10.66	23.33	89.45	384.45	9453	18.85	0.19
NDBC 41001	10.45	23.62	57.39	188.39	604.43	9729	38.83	0.39
WIS 41001	9.26	20.17	47.94	154.49	648.88	9440	33.05	0.34
NDBC 41002	8.72	18.69	42.99	149.27	906.36	10,132	32.62	0.32
WIS 41002	8.64	16.84	37.43	121.11	959.39	9937	29.52	0.30
NDBC 41010	6.49	12.86	28.23	100.88	557.85	10,322	22.35	0.22
WIS 41010	7.39	13.34	29.00	90.53	518.32	9828	21.23	0.21
NDBC 41009	3.71	7.71	17.43	59.91	428.99	11,091	13.96	0.13
WIS 41009	5.52	9.65	20.73	61.82	345.55	10,597	13.81	0.13

Standard deviations across a number of the reviewed Atlantic sites are generally comparable to the 90th percentile wave power estimates, and not the median or mean wave power calculations (Table 5). These results are due to the locally generated wind sea wave conditions with localised extreme events that are experienced at these sites. Standard errors across the reviewed sites remain low (Table 5), again allowing for confidence in these calculations.

As at the eastern Pacific Ocean sites, linear regression trends within the Atlantic Ocean vary across the spectrum of NDBC sites (Fig. 9) with environmental forcing variations. After removal of seasonal effects, NDBC daily mean wave power trends, ranging from 5 to 35 kW/m within the Atlantic Ocean, show agreement in mean daily wave power peaks and troughs, if not wave power magnitude, across each site (Fig. 9).

These wave power trends appear to follow trends in both NAO and ENSO LOWESS regressions, where peaks are evident within both climate indices and NDBC stations 44005, 41001 and 41002 between 1982 and 1984 (Fig. 9). Trends in wave power peaks at NDBC stations 41001 and 41002 correspond to NAO peaks in 1989, while peaks at all but one of the NDBC stations match the NAO peak in 1999 (Fig. 9). Peaks in wave power at NDBC stations 44008, 44011, 41001 and 41002

appear aligned with a peak in ENSO trends in 1986–1987, with all NDBC stations showing a peak in line with the ENSO peak in the 1998 timeframe, and again in 2015 (Fig. 9).

Of interest is the universal peak in wave power across the NDBC station within 2005 that does not correspond to a peak in the NAO or ENSO indices (Fig. 9). This peak, however, clearly reflects the extremely active 2005 hurricane season that the Atlantic Ocean experienced (Appendix D), where the NHC recorded 31 tropical cyclones and depressions for the area. This seasonal intensity is only matched within the Atlantic Ocean by the recent 2020 hurricane season, which, unfortunately, is not fully captured within our dataset (Fig. 9). However, the 1995, 2003, 2010, 2011 and 2019 hurricane seasons all registered 20 or more storm events (NHC 2022; Appendix D), which are echoed in the trend peaks within Fig. 9.

The overarching objective of these plots is to notice that a number of NDBC stations are showing an upward linear regression trend across the 40-year reviewed period (Fig. 9), deviating from the previous, almost universal downward linear regression trends observed within the eastern Pacific Ocean. In fact, four (NDBC stations 41009, 44008, 44013 and 44014) of the ten Atlantic sites show upward trends for both seasonal and seasonally detrended trends over the

Fig. 9 NDBC wave power trends for the Atlantic Ocean, with concurrent LOWESS regressions of the reference NAO and ENSO indices for trend context (bottom plot)

time period (Fig. 9; Table 6), which are consistent with Ahn and Neary's (2020) Atlantic moored buoy inter-annual mean total wave power of 0.02 kW/m/year for NDBC station 44025 (a site not reviewed within this study due to a deployment period of less than 30 years). Interestingly, NDBC stations 44008 (0.175 kW/m/year) and 44011 (−0.025 kW/m/year), both situated on the coastal shelf in relatively close proximity (Fig. 1), return opposite non-detrended wave power trend results (Table 6).

All but three NDBC stations show upward trends that are statistically significant (*p*-value less than 0.05), with all of the WIS sites estimating upward trends for wave power that is seasonally detrended (Table 6). As expected with the offset in wave power, a higher number of WIS sites return significant trends; however, all sites exhibited a good NDBC-WIS Pearson correlation coefficient of 0.91 or higher (Table 2). No site-specific correlations for latitudinal (North to South) or longitudinal (East to West) wave power trends were detected.

3.5 Gulf of Mexico wave power

Of the reviewed regions and even with its famous hurricane-prone reputation, the Gulf of Mexico sites captures the least amount of wave power overall, with hourly maximums ranging from a low of 144.89 kW/m (*n* = 8659) at NDBC station 42019, to a high of 664 kW/m (*n* = 11,941) at NDBC station 42003 for the 39-year review period (Table 7). However, a large portion of the wave power is captured within the 99th percentile, which reaches a Gulf of Mexico maximum of 59.84 kW/m (*n* = 13,146) at NDBC station 42002

(Table 7). Within this region, median hourly wave power values are predominantly lower than the other regions, ranging between 2.29 kW/m (*n* = 11,941) at NDBC station 42003 (even though this station exhibits the highest maximum wave power within the region) to 4.02 kW/m (*n* = 9097) at NDBC station 42020 (Table 7).

These results are due to the smaller Gulf of Mexico body of water, where the background wave climate is predominantly composed of locally generated wind sea conditions, and minimal swells entering into the system through the Yucatan Channel or Florida Straits. NDBC station 42003 (Fig. 1) is the closest reviewed station to these channels to the Atlantic Ocean and is situated within the location of the oscillating Gulf Loop Current (Maul, 1977; Oey et al., 2005). NDBC stations 42020 and 42019 (Fig. 1) are on the continental shelf in the shadow of the US land mass that reduces open water area for local wind-wave development, which explains their minimal wave power values, although they are exposed to easterly and south-easterly wind-wave growth. NDBC station 42001 and 42002 (Fig. 1) are subjected to Loop Current eddies that break away from the main Loop Current and propagate westwards (Maul, 1977; Oey et al., 2005), introducing wave energy into the system through their clockwise rotations.

These various land and oceanographic influences on the wave climate within the Gulf of Mexico are evident in the mean daily wave power trends and linear regression trends over time (Fig. 10). However, significant hurricane events, Hurricane Katrina (August 2005; Knabb, 2005); Hurricane Rita (September 2005; NHC, 2022); and Hurricane Wilma (October 2005; NHC, 2022), passed over NDBC station

Table 6 Atlantic Ocean 40-year regression trends for each site (displayed from North to South) for non-detrended and seasonally detrended daily mean wave power (kW/m). Significant trends per year are indicated in bold (*p*-value < 0.05)

Station	Wave power trends (kW/m/yr.)	Wave power slope (kW/m/day)	Wave power intercept (kW/m)	NDBC/WIS Pearson correlation coefficient	Seasonally detrended wave power trends (kW/m/yr.)	Seasonally detrended wave power slope (kW/m/day)	Seasonally detrended wave power intercept (kW/m)	Seasonally detrended NDBC/WIS Pearson correlation coefficient	Number of samples
NDBC 44007	−0.007	−0.00002	5.855	0.91	−0.005	−0.00001	5.791	0.91	13,515
WIS 44007	**0.043**	0.00012	2.647		**0.044**	0.00012	2.611		
NDBC 44005	**−0.165**	−0.00045	18.332	0.93	**−0.159**	−0.00044	18.144	0.91	13,867
WIS 44005	−0.001	0.00000	8.803		0.002	0.00000	8.698		
NDBC 44013	**0.083**	0.00023	2.370	0.95	**0.084**	0.00023	2.329	0.95	11,689
WIS 44013	**0.072**	0.00020	0.721		**0.073**	0.00020	0.708		
NDBC 44011	−0.025	−0.00007	25.764	0.95	−0.012	−0.00003	25.382	0.94	12,784
WIS 44011	**0.164**	0.00045	14.024		**0.173**	0.00048	13.727		
NDBC 44008	**0.175**	0.00048	13.081	0.94	**0.184**	0.00050	12.817	0.93	13,150
WIS 44008	**0.209**	0.00057	8.608		**0.216**	0.00059	8.398		
NDBC 44014	0.028	0.00008	10.901	0.94	0.028	0.00008	10.936	0.93	10,593
WIS 44014	**0.091**	0.00025	7.533		**0.089**	0.00025	7.605		
NDBC 41001	−0.028	−0.00008	25.276	0.92	−0.015	−0.00004	24.870	0.91	14,564
WIS 41001	0.029	0.00008	19.595		**0.038**	0.00010	19.294		
NDBC 41002	**−0.060**	−0.00016	21.254	0.92	**−0.053**	−0.00015	21.040	0.91	14,094
WIS 41002	**0.102**	0.00028	14.286		**0.108**	0.00030	14.114		
NDBC 41010	−0.038	−0.00010	14.511	0.93	**−0.039**	−0.00011	14.543	0.92	11,323
WIS 41010	**0.094**	0.00026	10.508		**0.092**	0.00025	10.555		
NDBC 41009	0.026	0.00007	7.496	0.95	0.022	0.00006	7.623	0.95	11,323
WIS 41009	**0.139**	0.00038	5.688		**0.135**	0.00037	5.796		

Table 7 Gulf of Mexico hourly wave power (kW/m) descriptive statistics for each site (displayed from North to South, then West to East) for the reviewed 39-year period

Station	Median	Mean	90th percentile	99th percentile	Max.	Number of Obs.	Std. deviation	Std. error
NDBC 42019	3.52	6.46	15.29	42.65	144.89	8659	9.17	0.10
WIS 42019	2.61	5.49	13.17	38.70	407.63	8037	9.87	0.11
NDBC 42020	4.02	7.06	16.27	45.03	233.45	9097	10.29	0.11
WIS 42020	3.28	5.37	12.17	32.01	72.18	2237	6.42	0.14
NDBC 42002	3.34	7.40	18.04	59.84	310.63	13,146	12.75	0.11
WIS 42002	2.73	6.45	15.28	57.42	266.75	12,428	12.28	0.11
NDBC 42001	2.36	6.08	14.47	55.04	461.48	12,394	12.73	0.11
WIS 42001	2.02	5.51	13.14	50.48	365.26	12,118	12.06	0.11
NDBC 42003	2.29	5.87	13.92	50.05	664.00	11,941	13.14	0.12
WIS 42003	1.44	4.65	10.77	45.50	736.67	11,272	13.61	0.13

Fig. 10 NDBC wave power trends for the Gulf of Mexico. Peaks within the wave power trends did not appear similar to trends within the climate indices, and so are not included. The dramatic peak experienced during 2005 at NDBC station 42003 represents the increase in wave power as Hurricane Katrina moved over the buoy (orange box)
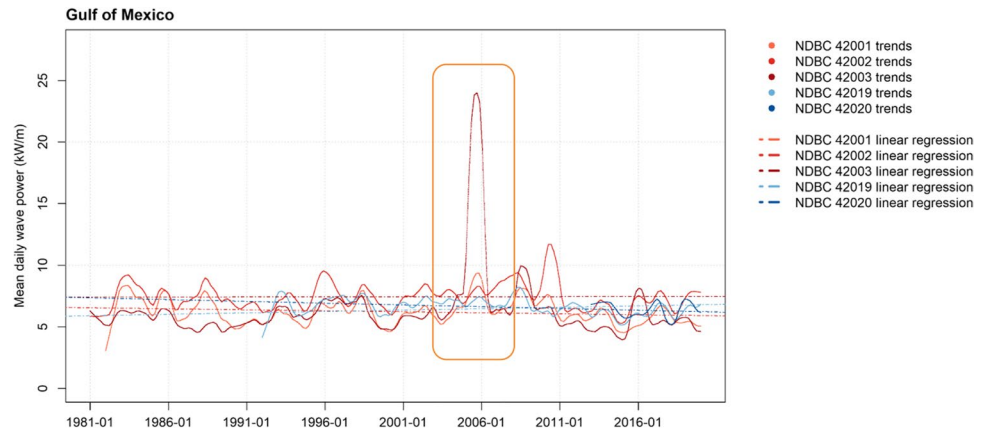
42003 with enough wave power to ensure their signals are represented in the seasonally detrended mean daily wave power (orange box in Fig. 10). Here the mean daily seasonally detrended wave power reaches 24 kW/m, far exceeding the background mean daily wave power trends that range within 5–12 kW/m for the then (prior to 2020) record-breaking 2005 hurricane season (Fig. 10). Of note is that the data signal evident for September 2005 is interpolated NDBC data, as the mooring at NDBC station 42,003 failed during Hurricane Katrina (August 28, 2005), before NDBC redeployment on October 6, 2005. These results provide yet another validation of the data methodology applied for these analyses.

The lower background wave power estimates are echoed within the non-detrended and seasonally detrended daily mean wave power regression trends in Table 8, where only one NDBC station (42019) shows both a statistically significant non-detrended (-0.030 kW/m/year; $n = 10,228$) and seasonally detrended (-0.029 kW/m/year) trend, and only one NDBC station (42001) shows a significant seasonally detrended trend (-0.016 kW/m/year; $n = 13,880$). These results show the benefits of reviewing variability between non-detrended and seasonally detrended wave power trends. Of note is that these smaller wave power trends show relative agreement with Ahn and Neary's (2020) NDBC station 42040 inter-annual mean total wave power results of 0.04 kW/m/year.

Table 8 Gulf of Mexico 39-year regression trends for each site (displayed from North to South) for non-detrended and seasonally detrended daily mean wave power (kW/m). Significant trends per year are indicated in bold (p-value < 0.05)

Station	Wave power trends (kW/m/yr.)	Wave power slope (kW/m/day)	Wave power intercept (kW/m)	NDBC/WIS Pearson correlation coefficient	Seasonally detrended wave power trends (kW/m/yr.)	Seasonally detrended wave power slope (kW/m/day)	Seasonally detrended wave power intercept (kW/m)	Seasonally detrended NDBC/WIS Pearson correlation coefficient	Number of samples
NDBC 42019	**−0.030**	−0.00008	7.705	0.86	**−0.029**	−0.00008	7.678	0.85	10,228
WIS 42019	**0.027**	0.00007	4.576		**0.027**	0.00008	4.545		
NDBC 42020	−0.022	−0.00006	7.455	0.93	−0.022	−0.00006	7.467	0.92	2557
WIS 42020	0.091	0.00025	1.453		0.090	0.00025	1.460		
NDBC 42002	0.000	0.00000	7.436	0.90	0.001	0.00000	7.409	0.89	14,245
WIS 42002	0.014	0.00004	6.140		0.014	0.00004	6.150		
NDBC 42001	−0.018	−0.00005	6.782	0.93	**−0.016**	−0.00005	6.744	0.93	13,880
WIS 42001	0.014	0.00004	5.237		0.014	0.00004	5.219		
NDBC 42003	0.022	0.00006	5.684	0.97	0.023	0.00006	5.657	0.97	14,245
WIS 42003	0.030	0.00008	4.520		0.030	0.00008	4.514		

Overall, of the five reviewed Gulf of Mexico NDBC stations, three stations returned downward mean power trends, and two stations returned upward trends per year (Table 8), regardless of seasonality. NDBC and WIS trends and slopes differ at all the sites with downward trends per year at the collocated locations, due to the low wave energy environment. However, all sites exhibited reasonable NDBC-WIS Pearson correlation coefficients of 0.85 or higher (Table 8), even with the varying directional slope trends.

3.6 Regional 90% wave power

For coastal engineering and planning purposes (Forte et al., 2012), the non-detrended 90th percentile wave power results were annually aggregated across each region to isolate maximum values within the Atlantic Ocean, Gulf of Mexico, eastern Pacific Ocean and Hawaii (Fig. 11). These results show that those considering baseline wave power conditions within the eastern Pacific Ocean should expect the maximum 90th percentile of non-detrended for season wave power values to range between 414 and 1937 kW/m ($n = 43$ years), with standard errors (SE) from 45 to 175 kW/m respectively
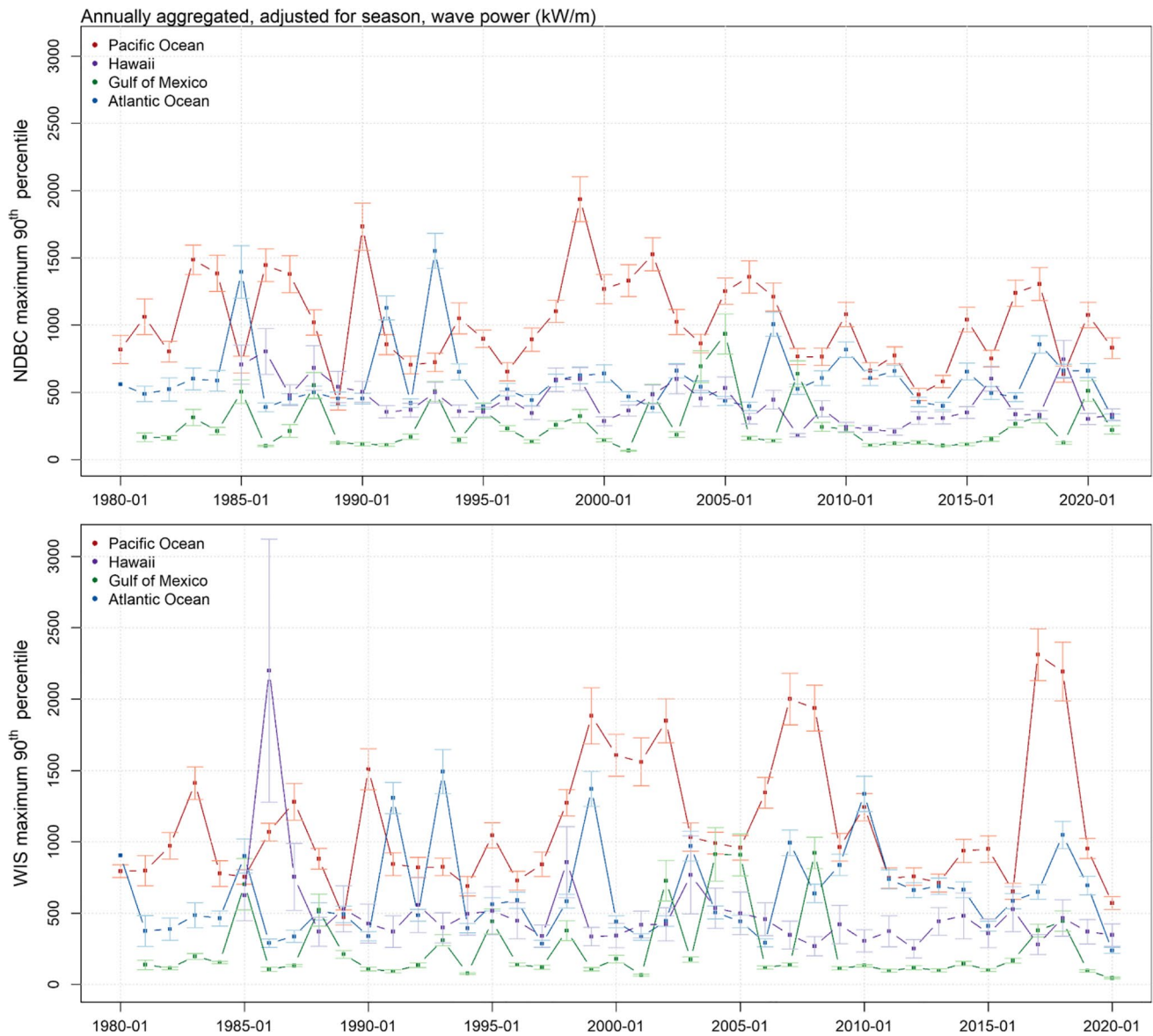

Fig. 11 Spatial and temporal variability in annually aggregated, non-detrended, maximum NDBC (top plot) and WIS (bottom plot) 90th percentile wave power (kW/m) across the Atlantic Ocean, Gulf of Mexico, eastern Pacific Ocean and Hawaii, with error bars representing the standard error

across the eastern Pacific Ocean NDBC stations (Fig. 11, top plot). Within the Atlantic Ocean, non-detrended for season wave power values are less intense, with maximum 90th percentile values ranging between 312 and 1551 kW/m (SE: 21–196 kW/m; $n = 42$ years) across the NDBC sites (Fig. 11, top plot). Moving further down the scale in wave power intensity, the Hawaiian NDBC sites (Fig. 11, top plot) show maximum 90th percentiles of non-detrended for season wave power values that range between 180 and 803 kW/m (SE: 12–171 kW/m; $n = 37$ years). Finally, the least intense reviewed wave power region, the Gulf of Mexico NDBC sites (Fig. 11, top plot), have recorded a maximum 90th percentile of non-detrended for season wave power values that range between 66 and 934 kW/m (SE: 3–148 kW/m; $n = 41$ years). Interestingly, the 2005 Gulf of Mexico hurricane season is represented as above the norm within the annual maximum 90th percentile (Fig. 11).

The WIS non-detrended for season, maximum 90th percentile wave power shows a larger range of 471–2311 kW/m (SE: 45–206 kW/m; $n = 41$ years) for the eastern Pacific Ocean sites, 240–1492 kW/m (SE: 20–155 kW/m; $n = 41$ years) for the Atlantic Ocean sites, 252–2200 kW/m (SE: 64–922 kW/m; $n = 36$ years) for the Hawaiian sites, and 47–923 kW/m (SE: 5–188 kW/m; $n = 40$ years) for the Gulf of Mexico sites. As before, the peaks of NDBC and WIS wave power estimates show agreement in the peaks over time, but magnitude differences between the two dataset persist within these results.

Therefore, the spatial and temporal variability between the NDBC and the WIS wave power estimates are evidenced by higher WIS wave power ranges for the eastern Pacific Ocean and Hawaiian Island sites, and comparable maximum 90th percentile wave power ranges for the Atlantic and Gulf of Mexico sites. Apart from the Hawaiian sites, standard errors appear relatively similar between the NDBC and the WIS wave power ranges. The annual maximum 90th percentile per region has a tendency to overshadow the individual buoy results, necessitating the calculation of site-specific wave power estimates for accurate assessments. However, while the investigation of wave power potential at individual sites requires a localised wave climate study for accurate planning and engineering purposes, these overall baseline wave power estimates will assist in initial project designs and development within each of the four regions.

4 Summary

In summary, buoy measurement data may be used to calculate wave power trends over time. Additionally, moored buoy wave power data are comparable with wave model wave power estimates; both showing that wave power trends are not increasing over time as appreciably as significant wave heights. Overall, the majority of the eastern Pacific Ocean and Hawaii wave power trends are downward, with mixed slope wave power trends apparent within the Atlantic Ocean and the Gulf of Mexico. As there is a noticeable variability in the trend direction within each reviewed region, site specific trends should not be generalised to represent a large region.

Wave power estimates differ from region to region due to area-specific wave conditions, with the eastern Pacific Ocean ranking as the more energetic of the regions with respect to wave power. After ranking by maximum wave power, 60% of the top ten stations are located along the eastern Pacific Ocean coastline. The Atlantic Ocean registers as the second most energetic coastline within these reviewed sites, with Hawaii logging in at third place. The Gulf of Mexico contains the least amount of wave power with these regions, although the Gulf of Mexico wave power trends clearly highlight extreme weather events that affect the region.

The higher wave power values that are observed within the eastern Pacific Ocean are attributed to the swell-dominated, longer T_p conditions that those sites are exposed to. These conditions form from a combination of North Pacific storms that pass through between autumn and spring, as well as the southern swells from the South Pacific and the Southern Ocean that penetrate the region within the summer months. The Atlantic Ocean experiences lower T_p conditions due to a predominant wave climate of local wind seas with following swells from Nor'easters. For the southern Atlantic Ocean locations (south of Cape Hatteras), tropical cyclone activity is evident in spatially variable wave power values that are a factor of five lower than those observed within the eastern Pacific. Within the Hawaiian region, the northern versus southern sites showed a difference in wave power magnitude (higher in the north), highlighting the effect of the northern site's exposure to North Pacific storm swells, while the rest of the reviewed Hawaiian sites experienced central Pacific and Southern Ocean swell signals. While the Gulf of Mexico records the lowest wave power values across the four reviewed regions due to its wind sea conditions and smaller area, the net impact of extreme events is evident within the background wave power estimates.

Overall, all of the reviewed regions produced daily mean wave power trends that show associations with extreme tropical weather events that were recorded by the NHC (1995–2021). Peaks in wave power trends throughout the eastern Pacific Ocean, Hawaiian and Atlantic Ocean sites appear to follow trends in both concurrent and variable PDO, NAO and ENSO LOWESS regressions. However, correlation does not infer causation and without in-depth analyses into the relationships between these wave power trends, and the reviewed climate indices, no definitive results are available here.

Finally, as the majority of wave power trend analyses and coastal engineering wave climate risk assessments are performed using wave model datasets, one of the objectives of this work was to quantitatively assess the differences between these model and observational data sources. Results show significant differences between the NDBC moored buoy and wave model wave power results that highlight the importance of using site specific results to investigate wave power within regions. These NDBC and WIS differences may be due to the different spectral-band frequency ranges that are used to calculate the bulk wave parameters required for these wave power calculations. They also highlight the importance of using wave power over individual bulk parameters to evaluate the performance of the WIS modelling

technology. As this is the first study to use wave power as a metric to evaluate wave model results, there is reason for additional investigation to identify potential deficiencies in wind forcing or modelling technology.

In conclusion, moored buoy data are successfully accessed to investigate wave power trends within four coastal regions around the US. While observational and model results are relatively similar, the moored buoy data presents smaller wave power ranges for two of the four regions, suggesting that observational data are essential in local wave climate studies to ensure accurate estimates for coastal planners and engineers.

Appendix A

NDBC and associated WIS Stations, water depth and length of record

Eastern Pacific Ocean				Atlantic Ocean			
NDBC			Corresponding WIS Station	NDBC			Corresponding WIS Station
Station	# years	Depth (m)		Station	# years	Depth (m)	
46001	42	4054	46001	41001	42	4486	41001
46002	42	3455	46002	41002	42	3759	41002
46005	42	2852	46005	41009	32	42	41009
46006	41	4323	46006	41010	32	890	41010
46011	40	464.8	46011	44005	41	176.8	44005
46012	40	208.8	46012	44007	38	49	44007
46013	39	123.4	46013	44008	38	68.9	44008
46022	38	419	46022	44011	36	91.1	44011
46025	38	890	46025	44013	36	64.6	44013
46029	36	131	46029	44014	30	47	44014
Gulf of Mexico				Hawaii			
NDBC			Corresponding WIS point	NDBC			Corresponding WIS point
Station	# years	Depth (m)		Station	# years	Depth (m)	
42001	42	3194	42101	51001	39	4895	81310
42002	42	3088	42102	51002	36	4948	81301
42003	42	3265	42103	51003	36	1987	-
42019	30	83.5	42019	51004	36	5183	-
42020	30	84.1	42020				

Appendix B

Historical NDBC Payloads and Wave Measurement Systems

NDBC Payloads (NDBC 2003)	
GSBP	General Service Buoy Payload
MARS	Multifunction Acquisition and Reporting System
DACT	Data Acquisition and Control Telemetry
VEEP	Value Engineered Environmental Payload
AMPS	Advance Modular Payload System
ARES	Acquisition and Reporting Environmental System
SCOOP	Self-Contained Ocean Observing Payload

Historical NDBC Wave Systems and sampling information (NDBC 2003, 2018a; Teng et al. 2009)

Wave system	Record length	Sampling rate	N	Frequency range	Frequency band width
Wave Data Analyser (WDA)	20 min (1200 s)	1.50 Hz		0.02 to 0.50 Hz	0.01 Hz
Wave Analyser (WA)	20 min (1200 s)	2.56 Hz		0.03 to 0.40 Hz	0.01 Hz
Digital Wave Analyser (DWA)	20 min (1200 s)	2.00 Hz		0.00 to 0.40 Hz	0.01 Hz
Magnetometer Only Directional Wave Analyser (DWA-MO)	20 min (1200 s)	2.00 Hz		0.03 to 0.40 Hz	0.01 Hz
Wave Processing Module (WPM)	40 min (2400 s)	1.7066 Hz		0.0200–0.4850 Hz	0.0200 Hz (noise band): 0.010 Hz bandwidth 0.0325–0.0925 Hz: 0.005 Hz bandwidth 0.1000–0.3500 Hz: 0.010 Hz bandwidth 0.3650–0.4850 Hz: 0.020 Hz
Directional Wave Processing Module (DWPM)	20 min (1200 s)	1.7066 Hz		0.0200–0.4850 Hz	0.0200 Hz (noise band): 0.010 Hz bandwidth 0.0325–0.0925 Hz: 0.005 Hz bandwidth 0.1000–0.3500 Hz: 0.010 Hz bandwidth 0.3650–0.4850 Hz: 0.020 Hz
Non-Directional Wave Processing Module (NDWPM)	20 min (1200 s)	1.7066 Hz		0.0200–0.4850 Hz	0.0200 Hz (noise band): 0.010 Hz bandwidth 0.0325–0.0925 Hz: 0.005 Hz bandwidth 0.1000–0.3500 Hz: 0.010 Hz bandwidth 0.3650–0.4850 Hz: 0.020 Hz
Digital Directional Wave Module (DDWM)	20 min (1200 s)	1.7066 Hz		0.0200–0.4850 Hz	0.0200 Hz (noise band): 0.010 Hz bandwidth 0.0325–0.0925 Hz: 0.005 Hz bandwidth 0.1000–0.3500 Hz: 0.010 Hz bandwidth 0.3650–0.4850 Hz: 0.020 Hz

Appendix C

NDBC: 38 frequency bands									
0.0300	0.0400	0.0500	0.0600	0.0700	0.0800	0.0900	0.1000	0.1100	0.1200
0.1300	0.1400	0.1500	0.1600	0.1700	0.1800	0.1900	0.2000	0.2100	0.2200
0.2300	0.2400	0.2500	0.2600	0.2700	0.2800	0.2900	0.3000	0.3100	0.3200
0.3300	0.3400	0.3500	0.3600	0.3700	0.3800	0.3900	0.4000		

NDBC: 47 frequency bands

0.0200	0.0325	0.0375	0.0425	0.0475	0.0525	0.0575	0.0625	0.0675	0.0725
0.0775	0.0825	0.0875	0.0925	0.1000	0.1100	0.1200	0.1300	0.1400	0.1500
0.1600	0.1700	0.1800	0.1900	0.2000	0.2100	0.2200	0.2300	0.2400	0.2500
0.2600	0.2700	0.2800	0.2900	0.3000	0.03100	0.3200	0.3300	0.3400	0.3500
0.3650	0.3850	0.4050	0.4250	0.4450	0.4650	0.4850			

WIS WAVEWATCH III® 29 frequency bands: Pacific and Atlantic Ocean

0.0350	0.0385	0.0424	0.0466	0.0512	0.0564	0.0620	0.0682	0.0750	0.0825
0.0908	0.0999	0.1098	0.1208	0.1329	0.1462	0.1608	0.1769	0.1946	0.2141
0.2355	0.2590	0.2849	0.3134	0.3447	0.3792	0.4171	0.4588	0.5047	

WIS WAM frequency bands: 28 Western Alaska and Gulf of Mexico

0.0314	0.0345	0.0380	0.0418	0.0459	0.0505	0.0556	0.0612	0.0673	0.0740
0.0814	0.0895	0.0985	0.1083	0.1192	0.1311	0.1442	0.1586	0.1745	0.1919
0.2111	0.2323	0.2555	0.2810	0.3091	0.3400	0.3740	0.4114		

Appendix D

Table 12 Annual counts of US National Hurricane Center and Central Pacific Hurricane Center Annual Tropical Cyclones and Depressions per year (sourced from NHC 2022)

Year	Atlantic Ocean	Eastern Pacific Ocean	Central Pacific Ocean
1995	20	11	1
1996	13	12	2
1997	9	19	9
1998	14	15	3
1999	16	14	3
2000	19	19	4
2001	17	17	4
2002	14	16	5
2003	21	16	2
2004	16	16	3
2005	31	16	3
2006	10	21	5
2007	17	15	2
2008	17	18	1
2009	11	20	3
2010	21	12	1
2011	20	13	0
2012	19	17	0
2013	15	18	3
2014	9	21	2
2015	12	22	5
2016	16	22	1
2017	19	20	0
2018	16	25	1
2019	20	21	1
2020	31	21	0
2021	13	14	0

Author contribution Candice Hall: conceptualisation, methodology, data curation, writing—original draft, formal analysis, investigation, validation, funding acquisition, project administration.

Robert Jensen: conceptualisation, writing—review and editing.
David Wang: conceptualisation, writing—review and editing.

Data availability The authors confirm that the data supporting the findings of this study are available within the article. Datasets analysed during the current study are stored on the Coastal and Hydraulics Laboratory Data Server Website (USACE ERDC 2022).

Declarations

Competing interest The authors declare no competing interests.

References

Allan J, Komar P (2000) Are Ocean Wave Heights Increasing in the Eastern North Pacific? Eos 81(47):561–576. https://doi.org/10.1029/EO081i047p00561-01

Ahn S, Neary VS (2020) Non-stationary historical trends in wave energy climate for coastal waters of the United States. Ocean Eng 216:108044. https://doi.org/10.1016/j.oceaneng.2020.108044

Appendini CM, Hernández-Lasheras J, Meza-Padilla R, Kurczyn JA (2018) Effect of climate change on wind waves generated by anticyclonic cold front intrusions in the Gulf of Mexico. Clim Dyn 51:3747–3763. https://doi.org/10.1007/s00382-018-4108-4

Bertin X, Prouteau E, Letetrel C (2013) A significant increase in wave height in the North Atlantic Ocean over the 20th century. Global Planet Change 106:77–83. https://doi.org/10.1016/j.gloplacha.2013.03.009

Cialone MA, Massey TC, Anderson ME, Grzegorzewski AS, Jensen RE, Cialone A, Mark DJ, Pevey KC, Gunkel BL, McAlpin TO, Nadal-Caraballo NC, Melby JA, Ratcliff JJ (2015) North Atlantic Coast Comprehensive Study (NACCS) Coastal Storm Model Simulations: Waves and Water Levels. ERDC/CHL TR-15-14. Vicksburg, MS: U.S. Army Engineer Research and Development Center. https://chs.erdc.dren.mil/Content/documents//Projects/USACE_NACCS/ERDC-CHL_TR-15-14_v2.pdf

Cleveland WS (1979) Robust Locally Weighted Regression and Smoothing Scatterplots. J Am Stat Assoc 74(368):829–836

Cleveland RB, Cleveland WS, McRae JE, Terpenning IJ (1990) STL: a seasonal-trend decomposition procedure based on loess. J Off Stat 6(1): 3–33. http://bit.ly/stl1990

De Livera AM, Hyndman RJ, Snyder RD (2011) Forecasting time series with complex seasonal patterns using exponential smoothing. J Am Statist Assoc 106:2011–496. https://doi.org/10.1198/jasa.2011.tm09771

Dobrynin M, Murawksy J, Yang S (2012) Evolution of the global wind wave climate in CMIP5 experiments. Geophys Res Lett 39 (L18606), https://doi.org/10.1029/2012GL052843

Earle MD, Steele KE, Hsu YL (1984) Wave spectra corrections for measurements of hull-fixed accelerometers. Oceans 1984:725–730. https://doi.org/10.1109/OCEANS.1984.1152234

Earle MD, Steele KE, Wang DWC (1999) Use of advanced directional wave spectra analysis methods. Ocean Eng 26:1421–1434. https://doi.org/10.1016/S0029-8018(99)00010-4

Forte MF, Hanson JL, Hagerman G (2012) North Atlantic wind and wave climate: observed extremes, hindcast performance, and extratropical recurrence intervals, 2012 Oceans: 1–10. https://doi.org/10.1109/OCEANS.2012.6404822

Friedman JH (1984a) SMART User's Guide. Laboratory for Computational Statistics, Stanford University Technical Report No.1. https://apps.dtic.mil/sti/citations/ADA148262

Friedman JH (1984b) A variable span scatterplot smoother. Laboratory for Computational Statistics, Stanford University Technical Report No.5. http://www.slac.stanford.edu/cgi-wrap/getdoc/slac-pub-3477.pdf

Furuichi N, Hibiya T, Niwa Y (2008) Model-predicted distribution of wind-induced internal wave energy in the world's oceans. J Geophys Res 113 (C09034). https://doi.org/10.1029/2008JC004768

Gemmrich J, Thomas B, Bouchard R (2011) Observational changes and trends in the Pacific wave records. Geophys Res Lett 38 (L22601). https://doi.org/10.1029/2011GL049518

Gravens MB, Sanderson DR (2018) Identification and Selection of Representative Storm Events from a Probabilistic Storm Data Base. ERDC/CHL CHETN-VIII-9. U.S. Army Engineer Research and Development Center, Vicksburg, MS. https://doi.org/10.21079/11681/26341

Hall C, Jensen R (2021) Utilizing Data from the NOAA National Data Buoy Center. ERDC/CHL CHETN-I-100. U.S. Army Corps of Engineers, Engineering Research and Development Center, Vicksburg, MS. https://doi.org/10.25607/OBP-1087

Hall C, Jensen R (2022) United States Army Corps of Engineers Coastal and Hydraulics Laboratory Quality-controlled, Consistent Measurement Archive. Sci Data 9(248). https://doi.org/10.1038/s41597-022-01344-z

Huppert KL, Perron JT, Ashton AD (2020) The influence of wave power on bedrock sea-cliff erosion in the Hawaiian Islands. Geology 48(5):499–503. https://doi.org/10.1130/G47113.1

Hyndman RJ, Athanasopoulos G (2018) Forecasting: principles and practice, 2nd edition, OTexts: Melbourne, Australia. OTexts.com/fpp2. Accessed on 06 January 2022. https://otexts.com/fpp2/

Hyndman R, Athanasopoulos G, Bergmeir C, Caceres G, Chhay L, O'Hara-Wild M, Petropoulos F, Razbash S, Wang E, Yasmeen F (2021) forecast: forecasting functions for time series and linear models, R package version 8.15. https://pkg.robjhyndman.com/forecast/

Jabbari A, Ackerman JD, Boegman L, Zhao Y (2021) Increases in Great Lake winds and extreme events facilitate interbasin coupling and reduce water quality in Lake Erie. Sci Rep 11:5733. https://doi.org/10.1038/s41598-021-84961-9

Kamranzad B, Etemad-Shahidi A, Chegini V (2016) Sustainability of wave energy resources in southern Caspian Sea. Energy 97:549–559

Kelley DE (2018) The oce Package. In: Oceanographic Analysis with R. Springer, New York, NY. https://doi.org/10.1007/978-1-4939-8844-0_3

Kelley DE, Clark C, Layton C (2021) oce: Analysis of Oceanographic Data. https://cran.r-project.org/web/packages/oce/index.html

Kendall M, Stuart A (1983) The advanced theory of statistics, Vol.3, Griffin. pp.410--414.

Knabb RD, Rhome JR, Brown DP (2005), Tropical Cyclone Report Hurricane Katrina U.S. National Oceanic and Atmospheric Administration, National Hurricane Center, National Data Buoy Center. https://www.nhc.noaa.gov/data/tcr/AL122005_Katrina.pdf

Koch SE, DesJardins M, Kocin PJ (1983) An interactive Barnes objective map analysis scheme for use with satellite and conventional data. J Appl Meteorol Climatol 22:1487–1503. https://doi.org/10.1175/1520-0450(1983)022/3C1487:AIBOMA/3E2.0.CO;2

Komar PD, Allan JC (2007) Higher waves along U.S. East Coast Linked to Hurricanes. EOS 88(30):301–308. https://doi.org/10.1029/2007EO300001

Komen GJ, Cavaleri L, Donelan M, Hasselmann K, Janssen PAEM (1994) The WAM Report: Dynamics and Modelling of Ocean Waves. Science 270(5234):320. https://doi.org/10.1126/science.270.5234.320.a

Leonardi N, Ganju NK, Fagherazzi S (2015) A linear relationship between wave power and erosion determines salt-marsh resilience to violent storms and hurricanes. PNAS 113(1):64–68. https://doi.org/10.1073/pnas.1510095112

Li N, García-Medina G, Cheung KF, Yang Z (2021) Wave energy resources assessment for the multi-modal sea state of Hawaii. Renewable Energy 174:1036–1055. https://doi.org/10.1016/j.renene.2021.03.116

Livermont EA, Miller JK, Herrington TO (2015) Trends and changes in the NDBC wave records of the U.S. East Coast, Proc. 14th International Workshop on Wave Hindcasting and Forecasting & 5th Coastal Hazard Symposium, Key West, FL, USA. http://waveworkshop.org/14thWaves/Presentations/B2_WAVES-Livermont/202015/20In/20Situ-/2016-9.pdf

Livermont EA, Miller JK, Herrington TO (2017) Correcting for changes in the NDBC wave records of the United States, Proc.1st International Workshop on Waves, Storm Surges, and Coastal Hazards, Liverpool, UK http://waveworkshop.org/15thWaves/Presentations/A3.pdf

Mantua NJ, Hare SR (2002) The Pacific decadal oscillation. Journal of Oceanography 58 (1): 35–44 https://link.springer.com/article/https://doi.org/10.1023/A:1015820616384

Marchand P, Gill D (2018) waver: calculate fetch and wave energy. R package version 0.2.1. https://github.com/pmarchand1/waver

Massey TC, Wamsley TV, Cialone MA (2011) Coastal storm modeling – system integration. ASCE 2011: Solutions to Coastal Disasters. https://ascelibrary.org/doi/pdf/ https://doi.org/10.1061/41185/28417/2910

Massey TC (2019) ERDC'S Coastal Storm Modeling System: South Atlantic Coast Study. 2nd International Workshop On Waves, Storm Surges And Coastal Hazards, Melbourne, Australia. http://waveworkshop.org/16thWaves/Presentations/JJ4/20Massey_CSTORM_Briefing_2019_WavesSurge_Australia.pdf

Maul G (1977) The annual cycle of the gulf loop current: Part 1: observations during a one-year time series. J Mar Res 35(1):29–47

Menéndez M, Méndez FJ, Losada I, Graham NE (2008) Variability of extreme wave heights in the northeast Pacific Ocean based on buoy measurements. Geophys Res Lett 35:L22607. https://doi.org/10.1029/2008GL035394

Mentaschi L, Vousdoukas MI, Voukouvalas E, Dosio A, Feyen L (2017) Global changes of extreme coastal wave energy fluxes triggered by intensified teleconnection patterns. Geophys Res Lett 44:2416–2426. https://doi.org/10.1002/2016GL072488

Mudelsee M (2019) Trend analysis of climate time series: a review of methods. Earth Sci Rev 190:310–322. https://doi.org/10.1016/j.earscirev.2018.12.005

NOAA National Data Buoy Center (NDBC) (2003) Nondirectional and directional wave data analysis procedure. NDBC Technical Document 03–01, U.S. National Oceanic and Atmospheric Administration, National Weather Service, National Data Buoy Center.

NOAA National Data Buoy Center (NDBC) (2018a) Description of NDBC wave spectra, U.S. National Oceanic and Atmospheric Administration. Accessed on 25 January 2022. https://www.ndbc.noaa.gov/wavespectra.shtml

NOAA National Data Buoy Center (NDBC) (2018b) How are significant wave height, dominant period, average period, and wave steepness calculated? U.S. National Oceanic and Atmospheric Administration. Accessed on 25 January 2022. https://www.ndbc.noaa.gov/wavecalc.shtml

NOAA National Center for Environmental Information (NCEI) (2021a) El Niño/Southern Oscillation (ENSO) U.S. National Oceanic and Atmospheric Administration. Accessed December 29, 2021a. https://www.ncdc.noaa.gov/teleconnections/enso/

NOAA National Center for Environmental Information (NCEI) (2021b) Pacific Decadal Oscillation (PDO). U.S. National Oceanic and Atmospheric Administration. Accessed December 29, 2021b. https://www.ncdc.noaa.gov/teleconnections/pdo/

NOAA National Center for Environmental Information (NCEI) (2021c) North Atlantic Oscillation (NAO). U.S. National Oceanic and Atmospheric Administration. Accessed December 29, 2021c. https://www.ncdc.noaa.gov/teleconnections/nao/

NOAA National Hurricane Center (NHC) (2022) 2021 Atlantic Hurricane Season. U.S. National Oceanic and Atmospheric Administration. Accessed on 30 January 2022. https://www.nhc.noaa.gov/data/tcr/index.php?season=2021&basin=atl

NOAA Physical Sciences Laboratory (PSL) (2021) Multivariate ENSO Index Version 2 (MEI.v2). U.S. National Oceanic and Atmospheric Administration. Accessed December 29, 2021. https://www.psl.noaa.gov/enso/mei

Odériz I, Silva R, Mortlock TR, Mori N (2020) El Niño-Southern Oscillation Impacts on Global Wave Climate and Potential Coastal Hazards. J Geophys Res: Oceans 125:e2020JC016464. https://doi.org/10.1029/2020JC016464

Oey LY, Ezer T, Lee HC (2005) Loop current, rings and related circulation in the Gulf of Mexico: a review of numerical models and future challenges. In: Circulation in the Gulf of Mexico: observations and models, Sturges W, Lugo-Fernandez A (Eds.). Geophysical Monograph Series 161 31–56.

Panchang V, Kwon Jeong C, Demirbilek Z (2013) Analyses of extreme wave heights in the Gulf of Mexico for offshore engineering applications. ASME J Offshore Mechanics Arctic Eng 135(3):031104. https://doi.org/10.1115/1.4023205

R Core Team (2021) R: a language and environment for statistical computing. R Foundation for Statistical Computing, Vienna, Austria. https://www.R-project.org/

Reguero BG, Losada IJ, Méndez FJ (2015) A global wave power resource and its seasonal, interannual and long-term variability. Appl Energy 148:366–380. https://doi.org/10.1016/j.apenergy.2015.03.114

Reguero BG, Losada IJ, Méndez FJ (2019) A recent increase in global wave power as a consequence of oceanic warming. Nat Commun 10:205. https://doi.org/10.1038/s41467-018-08066-0

Resio DT, Bratos SM, Thompson EF (2003) Meteorology and wave climate, Chapter II-2. Coastal engineering manual. US Army Corps of Engineers, Washington DC, pp.72.

Riley R, Teng C, Bouchard R, Dinoso R, Mettlach T (2011) Enhancements to NDBC's Digital Directional Wave Module. OCEANS'11 MTS/IEEE KONA, Waikoloa, HI, 2011, 1–10. https://doi.org/10.23919/OCEANS.2011.6107025

Riley R, Bouchard RH (2015) An accuracy statement for the buoy heading component of NDBC directional wave measurements. The Twenty-fifth International Ocean and Polar Engineering Conference, Kona, Hawaii, USA, June 2015. Paper Number: ISOPE-I-15–497.

RStudio Team (2021) RStudio: integrated development for R. RStudio, Inc., Boston, MA. http://www.rstudio.com/

Ruggiero P, Komar PD, Allan JC (2010) Increasing wave heights and extreme value projections: the wave climate of the US Pacific Northwest. Coastal Eng 57(5):539–552. https://doi.org/10.1016/j.coastaleng.2009.12.005

Saha S, Moorthi S, Pan H et al (2010) The NCEP Climate Forecast System Reanalysis. Bull Am Meteor Soc. https://doi.org/10.1175/2010BAMS3001.1

Soares CG, Bento AR, Gonçalves M, Silva D, Martinho P (2014) Numerical evaluation of the wave energy resource along the Atlantic European coast. Computers and Geosciences 71:0098–3004. https://doi.org/10.1016/j.cageo.2014.03.008 (**ISSN 0098-3004**)

Steele KE, Lau JC, Hsu YL (1985) Theory and application of calibration techniques for an NDBC directional wave measurements buoy. IEEE Journal of Oceanic Engineering, OE-10(4). https://ieeexplore.ieee.org/stamp/stamp.jsp?arnumber=1145116

Steele KE, Teng C, Wang DWC (1992) Wave direction measurements using pitch-roll buoys. Oceanic Eng 19(4):349–375

Steele KE (1997) Ocean current kinematic effects on pitch–roll buoy observations of mean wave direction and nondirectional spectra. J Atmos Oceanic Tech 14(2):278–291

Stopa JE, Cheung KF, Chen YL (2011) Assessment of wave energy resources in Hawaii. Renew Energy 36(2):554–567. https://doi.org/10.1016/j.renene.2010.07.014

Storlazzi CD, Elias EPL, Berkowitz P (2015) Many Atolls May be Uninhabitable Within Decades Due to Climate Change. Sci Rep 5:14546. https://doi.org/10.1038/srep14546

Suzuki T, Kuriyama Y (2014) The effects of offshore wave energy flux and longshore current velocity on medium-term shoreline change at Hasaki. Japan Coastal Eng J 56(2):1450007–1450011. https://doi.org/10.1142/S0578563414500077

Teng C, Bouchard R, Riley R, Mettlach T, Dinoso R, Chaffin J (2009) NDBC's Digital Directional Wave Module. OCEANS 2009, Biloxi, MS, 1–8, https://doi.org/10.23919/OCEANS.2009.5422386

Ulazia A, Penalba M, Ibarra-Berastegui G, Ringwood J (2017) Wave energy trends over the Bay of Biscay and the consequences for wave energy converters. Energy 141:624–634. https://doi.org/10.1016/j.energy.2017.09.099

US Army Corps of Engineers (USACE) (2002) U.S. Army Corps of Engineers Coastal Engineering Manual – Part II, CECW-CE EM1110–2–1100.

US Army Corps of Engineers (USACE) Engineer Research and Development Center (ERDC) (2020) Wave Information Studies. Accessed 26 June 2020. http://wis.usace.army.mil/; http://wis.usace.army.mil/wis_documentation.html

US Army Corps of Engineers (USACE) Engineer Research and Development Center (ERDC) (2022). Coastal and Hydraulics Laboratory Data Server Website. https://chldata.erdc.dren.mil/

Wang DW, Liu AK, Peng CY, Meindl EA (1994) Wave-current interaction near the Gulf Stream during the surface wave dynamics experiment. J Geophys Res: Oceans 99(C3):5065–5079

The WAVEWATCH III Development Group (WW3DG) (2019): User manual and system documentation of WAVEWATCH III R version 6.07. Tech. Note 333, NOAA/NWS/NCEP/MMAB, College Park, MD, USA, 465 pp. +Appendices. https://raw.githubusercontent.com/wiki/NOAA-EMC/WW3/files/manual.pdf

Wu L, Qin J, Wu T, Li X (2018) Trends in global ocean surface wave characteristics as represented in the ERA-Interim wave reanalysis for 1979–2010. J Mar Sci Technol 23:2–9. https://doi.org/10.1007/s00773-017-0450-1

Young IR, Zieger S, Babanin AV (2011) Global trends in wind speed and wave height. Science 332:451–455. https://doi.org/10.1126/science.1197219

Young IR, Ribal A (2019) Multiplatform evaluation of global trends in wind speed and wave height. Science 364:548–552. https://www.science.org/doi/epdf/ https://doi.org/10.1126/science.aav9527

Zar JH (1984) Biostatistical analysis, 2nd edition, Prentice-Hall, Englewood Cliffs, New Jersey. ISBN 0-13-077925-3